


RESEARCH ARTICLE | *Neural Circuits*

# Volitional control of single-electrode high gamma local field potentials by people with paralysis

 Tomislav Milekovic,<sup>1,2,3</sup> Daniel Bacher,<sup>2,4</sup> Anish A. Sarma,<sup>2,4,5</sup> John D. Simeral,<sup>5,2,4</sup> Jad Saab,<sup>2,4</sup> Chethan Pandarinath,<sup>10,11,12</sup> Blaise Yvert,<sup>1,2,6</sup> Brittany L. Sorice,<sup>7</sup> Christine Blabe,<sup>10</sup> Erin M. Oakley,<sup>7</sup> Kathryn R. Tringale,<sup>7</sup> Emad Eskandar,<sup>8,9</sup> Sydney S. Cash,<sup>7,9</sup> Krishna V. Shenoy,<sup>11,12,13,14,15\*</sup> Jaimie M. Henderson,<sup>10,12,16\*</sup> Leigh R. Hochberg,<sup>5,2,4,7,9</sup> and John P. Donoghue<sup>5,1,2</sup>

<sup>1</sup>Department of Neuroscience, Brown University, Providence, Rhode Island; <sup>2</sup>Carney Institute for Brain Science, Brown University, Providence, Rhode Island; <sup>3</sup>Department of Fundamental Neuroscience, Faculty of Medicine, University of Geneva, Geneva, Switzerland; <sup>4</sup>School of Engineering, Brown University, Providence, Rhode Island; <sup>5</sup>Center for Neurorestoration and Neurotechnology, Rehabilitation Research & Development Service, Department of Veterans Affairs, Providence, Rhode Island; <sup>6</sup>Inserm, University of Grenoble, Cinatec-Lab U1205, Grenoble, France; <sup>7</sup>Department of Neurology, Massachusetts General Hospital, Boston, Massachusetts; <sup>8</sup>Department of Neurosurgery, Massachusetts General Hospital, Boston, Massachusetts; <sup>9</sup>Harvard Medical School, Boston, Massachusetts; <sup>10</sup>Department of Neurosurgery, Stanford University, Stanford, California; <sup>11</sup>Department of Electrical Engineering, Stanford University, Stanford, California; <sup>12</sup>Stanford Neurosciences Institute, Stanford University, Stanford, California; <sup>13</sup>Neurosciences Program, Stanford University, Stanford, California; <sup>14</sup>Department of Neurobiology, Stanford University, Stanford, California; <sup>15</sup>Department of Bioengineering, Stanford University, Stanford, California; and <sup>16</sup>Department of Neurology and Neurological Sciences, Stanford University, Stanford, California

Submitted 26 February 2018; accepted in final form 3 February 2019

Milekovic T, Bacher D, Sarma AA, Simeral JD, Saab J, Pandarinath C, Yvert B, Sorice BL, Blabe C, Oakley EM, Tringale KR, Eskandar E, Cash SS, Shenoy KV, Henderson JM, Hochberg LR, Donoghue JP. Volitional control of single-electrode high gamma local field potentials by people with paralysis. *J Neurophysiol* 121: 1428–1450, 2019. First published February 20, 2019; doi:10.1152/jn.00131.2018.—Intracortical brain-computer interfaces (BCIs) can enable individuals to control effectors, such as a computer cursor, by directly decoding the user's movement intentions from action potentials and local field potentials (LFPs) recorded within the motor cortex. However, the accuracy and complexity of effector control achieved with such “biomimetic” BCIs will depend on the degree to which the intended movements used to elicit control modulate the neural activity. In particular, channels that do not record distinguishable action potentials and only record LFP modulations may be of limited use for BCI control. In contrast, a biofeedback approach may surpass these limitations by letting the participants generate new control signals and learn strategies that improve the volitional control of signals used for effector control. Here, we show that, by using a biofeedback paradigm, three individuals with tetraplegia achieved volitional control of gamma LFPs (40–400 Hz) recorded by a single microelectrode implanted in the precentral gyrus. Control was improved over a pair of consecutive sessions up to 3 days apart. In all but one session, the channel used to achieve control lacked distinguishable action potentials. Our results indicate that biofeedback LFP-based BCIs may potentially contribute to the neural modulation necessary to obtain reliable and useful control of effectors.

\* K. V. Shenoy and J. M. Henderson contributed equally.

Address for reprint requests and other correspondence: T. Milekovic, Department of Basic Neuroscience, Faculty of Medicine, University of Geneva, Campus Biotech, 9 chemin des Mines, 1202 Geneva, Switzerland (e-mail: tomislav.milekovic@unige.ch).

**NEW & NOTEWORTHY** Our study demonstrates that people with tetraplegia can volitionally control individual high-gamma local-field potential (LFP) channels recorded from the motor cortex, and that this control can be improved using biofeedback. Motor cortical LFP signals are thought to be both informative and stable intracortical signals and, thus, of importance for future brain-computer interfaces.

biofeedback; brain-computer interface; local field potentials; motor cortex; people with tetraplegia

## INTRODUCTION

Brain-computer interfaces (BCIs) are being developed to provide individuals with paralysis with the ability to control an external effector, such as a computer cursor or a robotic limb, using their cortical neural activity (Ajiboye et al. 2017; Andersen et al. 2010, 2014; Bowsher et al. 2016; Chaudhary et al. 2016; Donoghue 2002; Donoghue et al. 2007; Gilja et al. 2011; Green and Kalaska 2011; Hochberg 2008; Hu et al. 2016; Kao et al. 2014; Miralles et al. 2015; Nicolelis and Lebedev 2009; Schroeder and Chestek 2016; Schwartz et al. 2006; Shenoy and Carmena 2014; Tsu et al. 2015; Wolpaw and Wolpaw 2012). The majority of BCI studies have used a biomimetic approach to provide participants with effector control (Fagg et al. 2007; Jackson and Fetz 2011). In this approach, modulations of neural activity recorded during imagined, attempted, or executed movements are then used to calibrate a decoder that maps the neural activity to the movements. During BCI use, the effector is driven by movements decoded from the neural activity, e.g., decoded movements to the left move the com-

puter cursor leftward. In an alternate biofeedback approach, the decoder is calibrated taking only the statistics of neural signals into account, without relying on any relationship between participants' intended movements and their neural activity (Fetz 2007; Jackson and Fetz 2011). The subjects are given feedback on the effector's position and then adapt their control strategies and, potentially, their neural activity, to generate desired effector movements (Basmajian 1963; Birbaumer et al. 1999; Engelhard et al. 2013; Fetz 1969; Ganguly and Carmena 2009; Gharabaghi et al. 2014; Hall et al. 2014; Hwang et al. 2013; Jarosiewicz et al. 2008; Kübler et al. 1999; Moritz and Fetz 2011; Moritz et al. 2008; Nishimura et al. 2013; Sollfrank et al. 2016; Vansteensel et al. 2016; Vukelić and Gharabaghi 2015; Weyand et al. 2015). While the adaptation process of the biofeedback approach may take time, the choice of mapping between the neural activity and the effector movements may be used to lead the subjects toward generating novel control signals (Birbaumer et al. 1999; Engelhard et al. 2013; Gharabaghi et al. 2014; Hall et al. 2014; Kübler et al. 1999, 2005; Moritz and Fetz 2011; Weyand et al. 2015). For example, by providing the subjects with feedback of a single channel, activity may lead them toward learning to selectively control that single channel, while activity of others potentially remain unaffected. However, the number and the fidelity of the independent signals may be limited by the recording technique and the extent to which the recorded neural population can modify its activity (Sadler et al. 2014). In particular, recorded signals must be stable during the adaptation and BCI use to allow the users to benefit from the biofeedback approach (Ganguly and Carmena 2009; Hall et al. 2014). The effectiveness of biofeedback BCIs based on intracortical recordings remains to be examined in people with paralysis.

Some of the most promising biomimetic BCIs to date are based on the modulation of action potential rates based upon single or multiunit activity recorded using microelectrode arrays (MEAs) implanted in the motor cortex (Aflalo et al. 2015; Ajiboye et al. 2017; Bouton et al. 2016; Collinger et al. 2013; Gilja et al. 2015; Hochberg et al. 2012, 2006; Jarosiewicz et al. 2015; Pandarinath et al. 2017). While biofeedback BCIs based on single unit activity have been demonstrated in nonhuman primates (Fetz 1969; Fetz and Wyler 1973; Ganguly and Carmena 2009, 2010; Hall et al. 2014; Moritz and Fetz 2011; Moritz et al. 2008), difficulty in recording stable single unit activity signals (Barrese et al. 2013; Dickey et al. 2009; Leach et al. 2010; Perge et al. 2013; Polikov et al. 2005) poses challenges for their translation to clinical use. While extracting multiunit activity by thresholding can lead to stable signals in nonhuman primates (Chetek et al. 2011; Christie et al. 2015; Flint et al. 2013; Nuyujukian et al. 2014; Stavisky et al. 2015), loss of stability over similar time periods has been noted in humans (Perge et al. 2014). Partly in response, human BCI studies to date have opted to rebuild new neural decoders each day rather than attempt to maintain identifiable single or multiunit activity signals across days (Ajiboye et al. 2017; Bacher et al. 2015; Collinger et al. 2013; Gilja et al. 2015; Hochberg et al. 2006, 2012; Kim et al. 2008; Pandarinath et al. 2017; Wodlinger et al. 2015).

Local field potentials (LFPs) typically below 500 Hz, recorded by MEA, are thought to represent the summed spiking and synaptic activity of small neuronal populations in the vicinity of the recording electrode (Buzsáki et al. 2012; Eccles

1951; Kajikawa and Schroeder 2011; Katzner et al. 2009; Lorente de No 1947; Pesaran 2009; Xing et al. 2009). As in multiunit activity signals, nonhuman primate studies have shown that LFPs can be stable over long time periods (Flint et al. 2013, 2016; Stavisky et al. 2015; Wang et al. 2014). Our recent study demonstrated that LFP responses to movement attempts of people with tetraplegia can be stable over several months (Milekovic et al. 2018). Frequent micromovements of an MEA over time (Perge et al. 2013) may lead to larger stability of LFPs relative to single and multiunit activity recordings due to the larger recording sphere of the LFPs (~250  $\mu\text{m}$ ) (Katzner et al. 2009) when compared with single and multiunit activity signals (~100  $\mu\text{m}$ ) (Gold et al. 2006). While it is still unclear whether LFPs are more stable than single and multiunit activity signals in human participants (Ajiboye et al. 2012; Milekovic et al. 2018; Perge et al. 2014; Simeral et al. 2011), these factors motivate further investigation into whether biofeedback BCIs based on LFPs may benefit from their potentially higher stability.

It has been shown that nonhuman primates' volitional control of MEA-recorded LFPs can improve by using a biofeedback BCI (Engelhard et al. 2013; Hall et al. 2014). BCIs based on MEA-recorded LFPs could provide a stable platform to leverage biofeedback in clinical applications. A biofeedback approach could help the user gain increased volitional control over LFPs. Furthermore, independent volitional control over LFPs recorded on different electrodes could be used to gain control of multiple degrees of freedom. A milestone toward that goal is to demonstrate accurate one-dimensional volitional control of LFPs recorded on single electrodes gained through biofeedback.

In this study, we used a BCI as a tool to examine the properties of volitional LFP control gained through a biofeedback paradigm within and across days. We focused on using the LFPs recorded from a single electrode in motor cortex for continuous cursor control in a one-dimensional task. We hypothesized that people with tetraplegia could generate a novel BCI control signal permitting a cursor to hover over up to 10 distinct vertical locations on a screen using LFPs from a channel lacking identifiable spiking activity by leveraging a biofeedback paradigm (Fetz 2007). Furthermore, we hypothesized that the biofeedback paradigm could be used to further improve the ability of participants to control the cursor in this LFP-based BCI task.

Three individuals with tetraplegia, one with brain stem stroke and two diagnosed with amyotrophic lateral sclerosis (ALS), could volitionally control LFPs in the "gamma" frequency band recorded on one MEA electrode, hereafter referred to as "volitional LFP control." All three gained control of a cursor in one-dimension with sufficient accuracy to allow us to test two hypotheses using biofeedback: 1) the use of the biofeedback paradigm during a 1-h session increases the volitional LFP control; and 2) the use of the same signal (gamma LFP recorded on the same electrode) for cursor control in consecutive sessions separated by up to 3 days increases the volitional LFP control. We found that volitional LFP control did not change significantly over the course of one session. In contrast, volitional LFP control did improve significantly from the first session through the second performed up to 3 days after on both attempts (once in each of two participants). One of these participants performed another session 8 days later and

retained the increase in his volitional LFP control. Together, our results indicate that a biofeedback BCI can improve single-electrode LFP-based control. The observed performance improvements motivate further efforts to characterize volitional LFP control and biofeedback methods to enhance BCI stability and accuracy, two key features for clinical applications of BCI systems.

## METHODS

**Participants and recordings.** Three participants, identified as T2, T6, and T7, took part in this study (see Table 1 for detailed information). Each was enrolled in the ongoing BrainGate2 pilot clinical trial (<https://www.clinicaltrials.gov/ct2/show/NCT00912041>). After enrollment, T2 and T6 had one and T7 had two 96-electrode microelectrode arrays (Blackrock Microsystems, Salt Lake City, UT; Fig. 1A) placed in the hand area “knob” of the motor cortex (Yousry et al. 1997) of the left hemisphere, as previously described (Hochberg et al. 2006). Each implanted array was connected to an amplifier through a percutaneous pedestal fixed to the participant’s skull. Neuronal recordings were analog filtered (Butterworth band-pass filter with cutoff frequencies of 0.3 Hz and 7.5 kHz), digitized at 30 kilosamples/s with a 16-bit analog-to-digital converter, and then streamed to a local network. We refer to this digitized 30 kilosamples/s signal as the “wideband” recording later in the text. Other computers on the network stored, processed, and analyzed the wideband MEA recordings in real time and ran an application that presented a cursor control task. The movements of the cursor were based on the participant’s volitionally engaged motor cortical activity. In cursor control sessions, participants performed cursor control tasks over a period of up to 4 h (including breaks) during a single day. T2, T6, and T7 completed one, five, and nine cursor control sessions, respectively (Table 2). Sessions are described in this report by combining a participant’s subject code and the day after MEA implantation. Permission for these studies was granted by the US Food and Drug Administration (Investigational Device Exemption) and the Partners Healthcare/Massachusetts General Hospital, Providence VA Medical Center, and Stanford University Institutional Review Boards. Detailed descriptions of the core elements of the investigational BrainGate system have been provided previously (Hochberg et al. 2006; Simeral et al. 2011).

**Task.** The participants’ task was to control a computer cursor in the vertical dimension (up-down) to acquire presented targets. The position of the cursor was directly related to the neural activity recorded from one MEA electrode. Broadly, cursor control sessions consisted of two parts: 1) acquisition of baseline control, during which participants learned and explored different volitional control strategies by moving the cursor in the absence of targets; and 2) testing of control, during which we measured participants’ ability to volitionally control their neural signals by acquiring targets. Detailed description of the task follows.

During each session, participants performed between seven and fifteen 3- to 12-min blocks of a visual feedback task, interleaved with breaks lasting between 30 s and a couple of minutes, with occasional longer breaks for technical adjustments or as requested by the partic-

Table 1. *BrainGate 2 clinical trial participants who participated in this study at the day of the first session*

Participant	Age	Sex	Handedness	Medical Condition
T2	66	Male	Right	Tetraplegia and Anarthria caused by brain stem stroke
T6	51	Female	Right	Amyotrophic Lateral Sclerosis
T7	54	Male	Right	Amyotrophic Lateral Sclerosis

T2, T6, T7, individual participants.

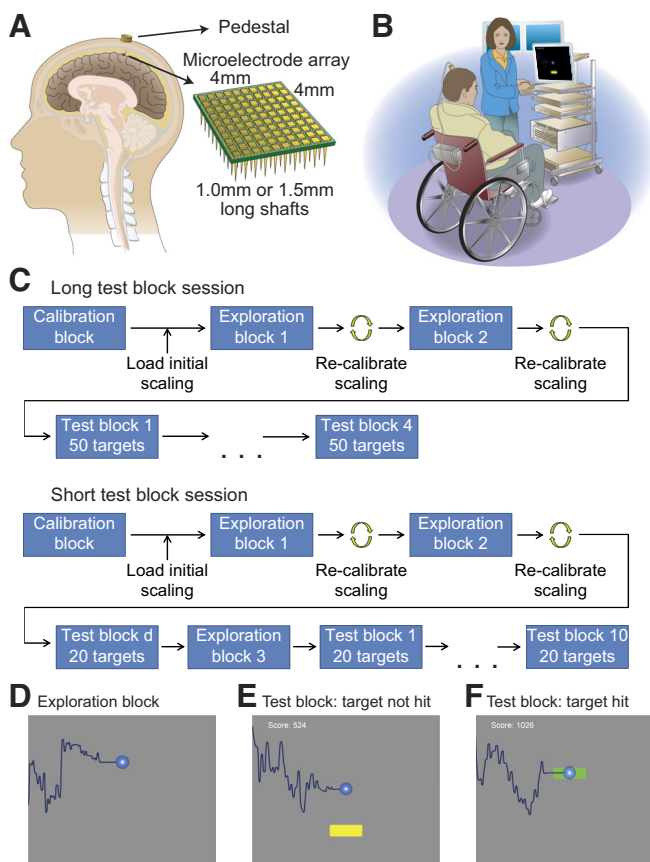


Fig. 1. Experimental setting and task design. **A:** participants were implanted with one (T2, T6) or two (T7) intracortical microelectrode arrays in the arm/hand area of the precentral sulcus of their left (dominant) hemispheres. An array covered an area of  $4 \times 4$  mm and consisted of 96 1.0-mm- or 1.5-mm-long electrodes. Neural recordings were transmitted by a wire bundle to a pedestal and then through a cable to an amplifier positioned on the participant’s wheelchair. **B:** sessions took place at each participant’s home, where the participant was comfortably seated in front of the computer monitor that showed the task. The technician attended the sessions, started and stopped tasks, and managed the session workflow. **C:** session design. Participants first observed the task without attempting any actions. The technician started the task in which she moved the cursor by moving the computer mouse while explaining the task to the participant (calibration block). After the calibration block, the technician calibrated the spectral amplitude normalization and loaded the initial scaling from the data file. The following two exploration blocks were each followed by a recalibration of the scaling. For long test block sessions, the second exploration block was followed by four consecutive long test blocks (50 targets). In short test block sessions, the second exploration block was followed by a dummy short test block (20 targets), another exploration block, and 10 consecutive short test blocks. During the exploration blocks (**D**), the participant would only see the current cursor position and its history (blue line). During the test blocks (**E** and **F**), the participant’s task was to touch the target with the cursor. When the cursor touched the target, it turned green (**F**); it was yellow otherwise (**E**). In **D**, **E**, and **F**, the black screen background seen by the participant is depicted gray to better illustrate the cursor trail.

ipants. The task was displayed on a computer monitor  $\sim 57$  cm (Fig. 1B) from the participants’ eyes. The monitor spanned  $\sim 37 \times 30^\circ$  of visual angle ( $38 \times 30$  cm) and each centimeter on the monitor was equivalent to  $\sim 1^\circ$  of visual angle. During all blocks, a cursor (blue sphere with radius of 5% of the monitor height;  $\sim 1.5^\circ$  of visual angle) and a blue “trail” displaying the most recent positions of the cursor were shown on the screen (Fig. 1D, Supplemental Movies S1 and S2; Supplemental Material for this article is available online at the Journal

Table 2. List of sessions and corresponding signal processing parameters

Session	STFT Window Length	Frequency Band	LWMA Filter Length	Session Type	
				Test blocks	Delay
T2 day 502	256 ms	52.73–193.36 Hz	800 ms	Long	Long
T6 day 322	256 ms	56.64–208.98 Hz	800 ms	Long	Long
T6 day 403	128 ms	58.59–207.03 Hz	400 ms	Long	Short
T6 day 451	256 ms	56.64–275.39 Hz	800 ms	Long	Long
T6 day 453	256 ms	56.64–275.39 Hz	800 ms	Long	Long
T6 day 493	128 ms	50.78–277.34 Hz	400 ms	Long	Short
T7 day 113	256 ms	44.92–216.80 Hz	800 ms	Long	Long
T7 day 158	256 ms	44.92–267.58 Hz	800 ms	Long	Long
T7 day 188	256 ms	52.73–220.70 Hz	800 ms	Short	Long
T7 day 195	256 ms	52.73–220.70 Hz	800 ms	Short	Long
T7 day 199	256 ms	44.92–373.05 Hz	800 ms	Short	Long
T7 day 202	256 ms	44.92–373.05 Hz	800 ms	Short	Long
T7 day 210	256 ms	44.92–373.05 Hz	800 ms	Short	Long
T7 day 223	128 ms	42.97–371.09 Hz	400 ms	Short	Short
T7 day 232	128 ms	42.97–371.09 Hz	400 ms	Short	Short

LWMA, linear weighted moving average; STFT, short-time Fourier transform; T2, T6, T7, individual participants.

website). The cursor could only move in the vertical dimension between the bottom and top edges of the screen (0 and 1 in screen coordinates, respectively). In a subset of the blocks (as described in the next paragraph), a target (rectangle with a height of 8.75% of the monitor height;  $\sim 2.6^\circ$  of visual angle) was also shown in one of 10 equally spaced locations centered at 10.25% of the monitor height ( $\sim 3^\circ$  of visual angle) to 89.75% of the monitor height ( $\sim 26.5^\circ$  of visual angle) from the bottom in steps of 8.83% of the monitor height ( $\sim 2.6^\circ$  of visual angle). Horizontally, the cursor and targets were always in the middle of the screen. The position of the target changed every 12, 10.16, and 10.52 s for T2, T6, and T7, respectively. The target turned green when the cursor was touching it, and was yellow otherwise (Fig. 1, *E* and *F*). In blocks that had targets, a score (*S*) was also displayed in the top left corner. To motivate the participant, the score increased when the cursor was touching the target according to the following equation:

$$S_t = \text{round}\left(0.0167 \cdot \sum_{\tau=1}^t D_\tau\right), D_\tau = \begin{cases} D_{\tau-1} + 1 & \text{if target hit} \\ 0 & \text{otherwise} \end{cases}$$

where *t* is the time step within the block. The precise temporal lengths of a time step slightly differed between participants and were on average 20, 17, and 17.6 ms for T2, T6, and T7, respectively, reflecting monitors with slightly different refresh rates at the various clinical trial sites. The blue trail showed the history of the cursor position over the last 600 time steps, corresponding to 12, 10.2, and 10.6 s for T2, T6, and T7.

The experimental design comprised three types of blocks: 1) calibration, 2) exploration, and 3) test blocks. Each session started with a calibration block ( $\sim 3$  min long), during which the technician controlled the cursor and described the task to the participant. The target was not presented for the first 30 s of the block and appeared at regular intervals afterward. The participants were asked to look at the screen, listen to the instructions, and not attempt any movements. Recordings from the calibration block were used to assess baseline neural activity. In all other blocks, the cursor position was determined from the participants' neural activity. The exploration blocks (each up to 12 min long) were designed to have the participants learn how attempted, imagined, or performed limb movements affect the cursor movements to reach some baseline level of cursor control. No targets were shown during the exploration blocks. During the first exploration block, the participants were instructed to attempt, perform, or imagine a variety of arm movements (hereafter termed "actions") read to them from a list by the technician (Table 3) and to observe the resulting cursor movements. After exploring an action for  $\sim 30$  s, the participants rated (on a scale of 1 to 10) their perceived quality of cursor

control. When all actions had been evaluated, the technician ended the block and each participant selected an action or a group of actions based on their rating and preferences. In the subsequent exploration blocks, the participants were asked to further explore variations of their selected actions to try to gain a better understanding of the relationship between their actions and cursor movements and, thereby, gain better control of the cursor. To further motivate participants, the technicians would occasionally ask them to try to move and keep the cursor in different locations on the screen (e.g., "Move the cursor up"; "Move the cursor down"). During test blocks, a target was always shown on the screen and the participants were instructed to bring the cursor in contact with the target as it changed positions to maximize their score (Fig. 1, *E* and *F*). The test blocks were designed to measure the level of participants' cursor control and to improve cursor control through the biofeedback paradigm. Specifically, by providing direct feedback of the neural activity and the related reward (in this case, a score), we aimed to reinforce neural activity that increases reward.

We conducted two types of sessions: 1) long test block sessions and 2) short test block sessions (Fig. 1C). T7 was the only participant who conducted short test block sessions, which were added at his request. Short test block sessions enabled him to be equally engaged at the task throughout the whole block, which he found difficult during long test blocks. In both session types, the participants saw a total of 200 targets during test blocks divided into either 50- or 20-target test blocks (long and short test blocks, respectively). In long and short test blocks, targets occupied each of 10 target positions five or two times, respectively. Therefore, the targets were distributed uniformly within each test block. Long test blocks lasted for 605, 513, and 531 s for T2, T6, and T7, respectively; and short test blocks lasted for 215.4 s (T7 only). The participants accumulated roughly the same amount of test block time irrespective of session type.

Each session started with a calibration block followed by two exploration blocks (Fig. 1C). During the first exploration block, we used initial scaling coefficients to convert neural features into the cursor position on the screen (see *Scaling calibration* for details). The scaling coefficients were recalibrated after the first and second exploration blocks based on the recordings from the first and second exploration block, respectively. In long test block sessions, the second exploration block was followed by four consecutive long test blocks. In all short test block sessions (participant T7 only), the second exploration block was followed by a "dummy" short test block, another (third) exploration block, and 10 consecutive short test blocks. In the dummy short test block, the participant was reminded of the task and encouraged to practice keeping the cursor in different positions of the screen for longer time periods. However, he was

Table 3. List of attempted and imagined movements that participants were instructed to perform during the first exploration block

All T2 and T6 Sessions	T7 Day 117	T7 Day 158	All Remaining T7 Sessions
<ul style="list-style-type: none"> <li>- Wiggle/move pinkie finger</li> <li>- Wiggle/move ring finger</li> <li>- Wiggle/move middle finger</li> <li>- Wiggle/move index finger</li> <li>- Wiggle/move thumb</li> <li>- Open–close hand</li> <li>- Flex/extend wrist</li> <li>- Abduct/adduct wrist (left–right)</li> <li>- Rotate wrist clockwise–counter clockwise</li> <li>- Flex–extend elbow (up–down)</li> <li>- Arm extended forward, move arm up–down</li> <li>- Arm extended to side, move arm up–down</li> <li>- Explore other movements as time permits</li> </ul>	<ul style="list-style-type: none"> <li>- Attempt to wiggle/move pinkie finger</li> <li>- Attempt to wiggle/move ring finger</li> <li>- Attempt to wiggle/move middle finger</li> <li>- Attempt to wiggle/move index finger</li> <li>- Attempt to wiggle/move thumb</li> <li>- Attempt to open–close hand</li> <li>- Attempt to flex/extend wrist</li> <li>- Attempt to abduct/adduct wrist (left–right)</li> <li>- Attempt to rotate wrist clockwise–counter clockwise</li> <li>- Attempt to flex–extend elbow (up–down)</li> <li>- Attempt to move the arm in different directions</li> <li>- Imagine to wiggle/move pinkie finger</li> <li>- Imagine to wiggle/move ring finger</li> <li>- Imagine to wiggle/move middle finger</li> <li>- Imagine to wiggle/move index finger</li> <li>- Imagine to wiggle/move thumb</li> <li>- Imagine to open–close hand</li> <li>- Imagine to flex/extend wrist</li> <li>- Imagine to abduct/adduct wrist (left–right)</li> <li>- Imagine to rotate wrist clockwise–counter clockwise</li> <li>- Imagine to flex–extend elbow (up–down)</li> <li>- Imagine to move the arm in different directions</li> <li>- Explore other movement attempts and movement imaginations as time permits</li> </ul>	<ul style="list-style-type: none"> <li>- Attempt to wiggle/move pinkie finger</li> <li>- Attempt to wiggle/move ring finger</li> <li>- Attempt to wiggle/move middle finger</li> <li>- Attempt to wiggle/move index finger</li> <li>- Attempt to wiggle/move thumb</li> <li>- Attempt combined movements of different fingers</li> <li>- Attempt to open–close hand</li> <li>- Attempt to move the wrist: flex/extend, abduct/adduct and rotate clockwise/counter clockwise</li> <li>- Attempt to move the arm in different directions by combining shoulder, elbow and wrist movements</li> <li>- Imagine to wiggle/move pinkie finger</li> <li>- Imagine to wiggle/move ring finger</li> <li>- Imagine to wiggle/move middle finger</li> <li>- Imagine to wiggle/move index finger</li> <li>- Imagine to wiggle/move thumb</li> <li>- Imagine combined movements of different fingers</li> <li>- Imagine to open–close hand</li> <li>- Imagine to move the wrist: flex/extend, abduct/adduct and rotate clockwise/counter clockwise</li> <li>- Imagine to move the arm in different directions by combining shoulder, elbow and wrist movements</li> <li>- Explore other movement attempts and movement imaginations as time permits</li> </ul>	<ul style="list-style-type: none"> <li>- Imagine to move different individual fingers</li> <li>- Imagine combined movements of different fingers</li> <li>- Attempt to open–close hand</li> <li>- Attempt to move the wrist: flex/extend, abduct/adduct and rotate clockwise/counter clockwise</li> <li>- Imagine to move the arm in different directions by combining shoulder, elbow and wrist movements</li> <li>- Attempt to move different individual fingers</li> <li>- Attempt combined movements of different fingers</li> <li>- Attempt to open–close hand</li> <li>- Attempt to move the wrist: flex/extend, abduct/adduct and rotate clockwise/counter clockwise</li> <li>- Attempt to move the arm in different directions by combining shoulder, elbow and wrist movements</li> <li>- Explore other movement attempts and movement imaginations as time permits</li> </ul>

T2, T6, T7, individual participants.

instructed not to try to maximize the score but rather to explore different actions. In the third exploration block, the participant was instructed to further explore different actions to achieve better cursor control.

As the session progressed, participants occasionally became less engaged with the task. We did not measure or systematically track participants' level of engagement, but, when observed or self-reported, we noted it in our session logs.

*Preprocessing of neural signals.* Our intention was to provide participants with volitional control of a single continuously modulated signal that contained movement-intention information but could not be used to immediately achieve a high level of accuracy in a complex one-dimensional task. We chose to use high-frequency-band LFPS recorded from a single electrode, since these signals have been found to modulate with movement directions (Mehring et al. 2003) and only simple BCI control has been achieved using LFPS recorded from two electrodes (Kennedy et al. 2000, 2004). In this section, we detail how we transformed wideband single-electrode recordings into a single continuously modulated signal that captured high-frequency LFP modulations.

Before each session, we selected an electrode based on the LFP modulations in the gamma band recorded during prior sessions (see *Selection of the electrodes and frequency bands used for cursor control* for details). Neural recordings were subsampled to 15 kilosamples/s to reduce the computational load for real-time processing and then common-average referenced to a subset of channels that contained the least amount of line noise (Fig. 2A). The number of channels in the subset was selected by the experimenter based on the distribution of line noise amplitudes over all channels. To further reduce the computational load of our real-time analysis, the signal from the single selected electrode was then further downsampled to 1 kilosamples/s by first applying a low-pass filter to control for aliasing effects (30 samples long windowed linear-phase finite impulse response filter with a 400-Hz cutoff frequency) and then taking every

15th sample. To estimate the spectral amplitudes of the signal, we used short-time Fourier transform (STFT; Allen 1977) with a window length of 128 ms (sessions *T6 day 403*, *T6 day 487*, *T7 day 223*, and *T7 day 232*) or 256 ms (all remaining sessions) and a Hamming window. We applied this STFT every 20 ms (temporal frequency of our software), which gave us spectral amplitude estimates in 3.91 or 7.82 Hz wide frequency bins, respectively. Similar window sizes were found to capture spectral amplitude modulations of intracortically recorded LFPS in people with paralysis during attempted movement (Perge et al. 2014). LFP spectral amplitudes become smaller with increasing frequency. To bring the amplitude modulations in different frequencies to a similar range, for each of the individual frequency bins, amplitude values were normalized by dividing by the mean amplitudes obtained during the calibration block. We then averaged the normalized amplitudes over frequency bins within a previously selected frequency band, which we referred to as the high-frequency selected band (HFSB) of LFPS (HFSB-LFP; see Table 2 for list of bands for each cursor control session and section *Selection of the electrodes and frequency bands used for cursor control* for a description of the selection procedure), thus obtaining one value for each of the selected electrodes every 20 ms. Distribution of HFSB-LFPs over time is skewed toward higher values. We transformed the spectral amplitudes using the natural logarithm, which made the HFSB-LFP distribution more symmetric. To reduce the high-frequency jitter of the signal, we then applied a linear weighted moving average (LWMA) filter (Yaffee and McGee 2000) with a 0.4-s (sessions *T6 day 403*, *T6 day 487*, *T7 day 223*, and *T7 day 232*) or 0.8-s (all remaining sessions) window (Fig. 2A), selected to provide a compromise between smooth and responsive cursor movements. This value was defined as the neural feature ( $f$ ) and was affine transformed using the scaling coefficients to get the position of the cursor on the screen during exploration and test blocks.

*Scaling calibration.* To maximize the use of biofeedback, modulations of the neural feature should map to cursor positions spanning

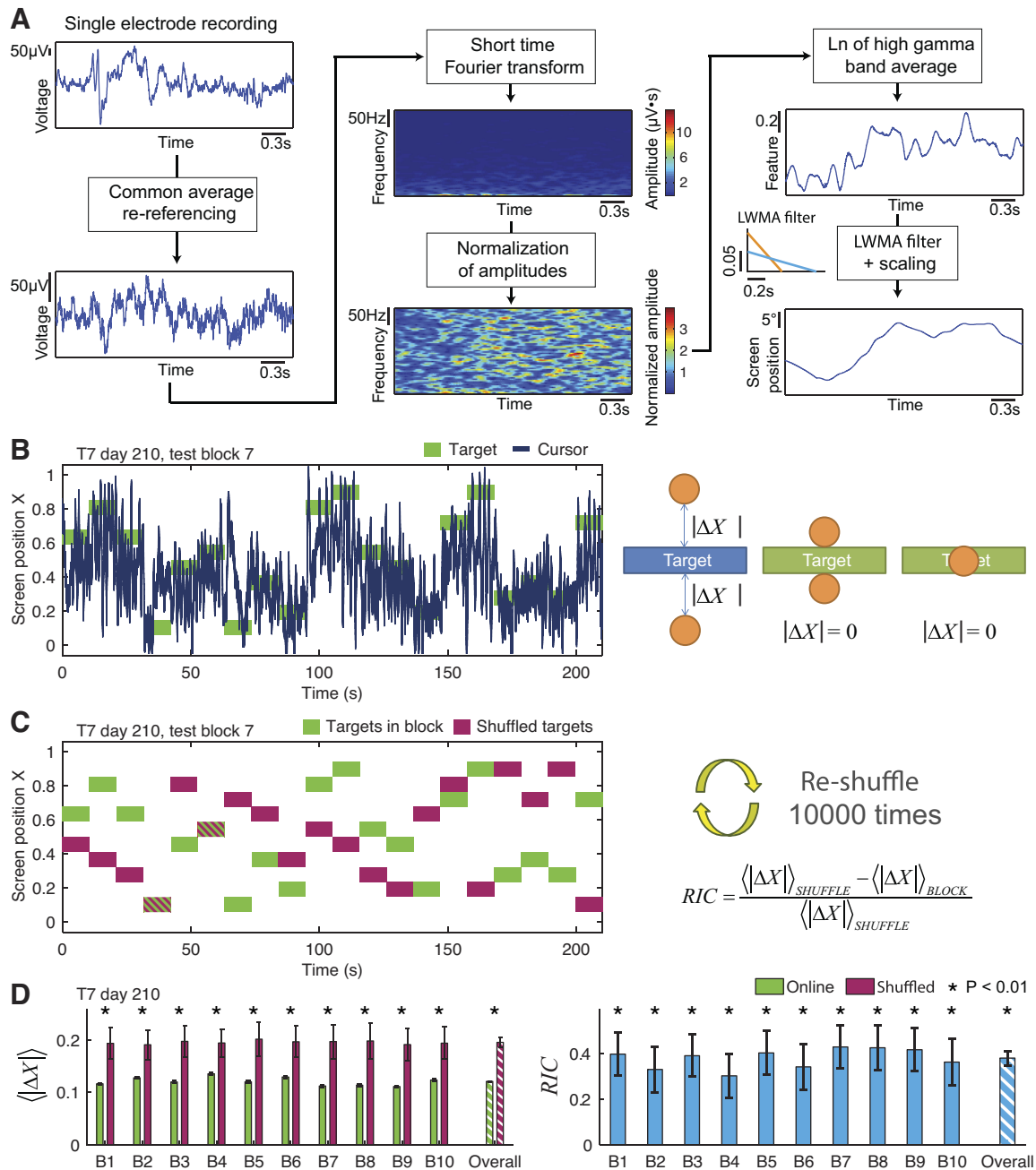


Fig. 2. Signal processing and the measure of participants' volitional high-frequency selected band of local field potential (HFSB-LFP) control. **A**: relationship of the neural activity to the cursor position on the screen. Voltage recordings from a single electrode were first common average referenced and then transformed into spectral amplitudes. Amplitudes in different frequency bins were normalized and averaged over the selected frequency band. The natural logarithm of the value was taken and filtered using a 0.8-s-long (blue line) or a 0.4-s-long (yellow line) linear weighted moving average (LWMA) filter to obtain the neural feature. The neural feature was then scaled to obtain the current cursor position. **B**: example of cursor and target positions in one of the short test blocks (*left*). Participant's ability to control the cursor was measured by the mean distance from the edge of the cursor to the edge of the target (*right*). If the cursor touched the target, the target was acquired and the distance for that time point was 0. **C**: the baseline performance was measured by calculating mean cursor edge-to-target edge distance for 10,000 random shuffles of the target positions (example of one shuffle shown at *left*). The participant's volitional control in relation to baseline was measured by calculating relative improvement in control (*RIC*). **D**: example of participant T7's volitional HFSB-LFP control performance for one of the sessions. *Left* shows mean cursor-edge-to-target-edge distance during the session (online, green histograms) and for shuffled targets (magenta histograms) for each test block (B1–B10) and overall. *Right*: *RIC* for each test block and overall. For this session, the participant had statistically significant control ( $P < 0.01$ , *t*-test) in every test block. \*Statistically significant *RIC* values.

most of the height of the screen (i.e., from 0 to 1). Conversely, incorrectly scaled or centered neural feature values would lead the cursor beyond the limits of the work space and would not be useful to capture targets. We found that modulation ranges of the neural features extracted from different electrodes and from the same electrode on different sessions varied substantially. Furthermore, modu-

lation range of the feature, and thus its optimal scaling, varied for different actions participants were using. Thus, we calibrated a new scaling for each session and recalibrated it two times within the session to estimate the optimal scaling for the participants' volitional control strategy. Here we describe the process of calibrating and recalibrating the scaling.

Table 4. List of sessions and participants' actions used to identify frequency bands that were used for cursor control during volitional local field potential control sessions

Session Used To Select the Frequency Band and Electrodes Used for Control of the Cursor	Action Performed by the Participant	Cursor Control Sessions that Used the Determined Frequency Band
T2 day 501	Attempt to close and then open right hand	T2 day 502
T6 day 313	Flex and then extend right index finger	T6 days 322 and 403
T6 day 440	Flex and then extend right index finger	T6 days 451, 453, and 493
T7 day 100	Attempt to close and then open right hand	T7 day 113
T7 day 118	Attempt to flex and then extend thumb	T7 day 158
T7 day 177	Attempt to flex and then extend right wrist	T7 days 188 and 195
T7 day 195	Attempt to flex and then extend right wrist	T7 days 199, 202, 210, 223, and 232

Participants T2, T6, and T7 performed the actions in response to visual cues. Note that sessions using the same frequency bands may use signal recorded from different electrodes for volitional control. Only sessions T6 days 451, 453, and 493 and T7 days 199, 202, 210, and 223 used the same electrode for volitional control.

Signals recorded on a single electrode were used for BCI control. The initial scaling coefficients were calculated from a prior session (same as for determining the HFSB; Table 4). From these sessions, we calculated the 5th and 95th percentiles of the neural feature from the selected electrode,  $f_{5\%}$  and  $f_{95\%}$ , respectively. To obtain the cursor position on the screen ( $X_{CURSOR}$ ), the neural feature was scaled as follows:

$$X_{CURSOR} = \frac{f - f_{5\%}}{f_{95\%} - f_{5\%}}$$

The scaling was recalibrated by calculating 5th and 95th percentiles of the neural feature in the first and second exploration block, respectively.

*Selection of the electrodes and frequency bands used for cursor control.* The frequency band and the electrodes used for control of the cursor were selected based on a prior session in which the participant was asked to perform an action in response to visual cues (Table 4). Detailed procedure is described under *Determining the electrodes and*

*frequency bands used for cursor control* in the APPENDIX. Briefly, we defined an action-relevant epoch following each visual cue and then calculated the frequency-band-specific signal-to-noise ratio ( $SNR_{FB}$ ) between these epochs and the remainder of the recording, defined as baseline, for each electrode. Except for session T7 day 100, maximum of electrode-averaged  $SNR_{FB}$  was used to determine the frequency band (Fig. 3). The electrode used for cursor control was selected among the electrodes with the highest  $SNR_{FB}$  for the selected frequency band. For session T7 day 100, we used the maximum of all single-electrode  $SNR_{FB}$  to select both the electrode and frequency band.

*Quantitative measures of volitional control.* To evaluate the initial level of volitional LFP control and the effects of biofeedback on that control, we designed a volitional control measure as follows. The participant's task was to initiate and maintain contact between the cursor and the target. Thus, we calculated the mean absolute edge-to-edge distance between the cursor and the target  $|\Delta X|$  (0 when cursor and target overlap) sampled every 20 ms over the whole test block

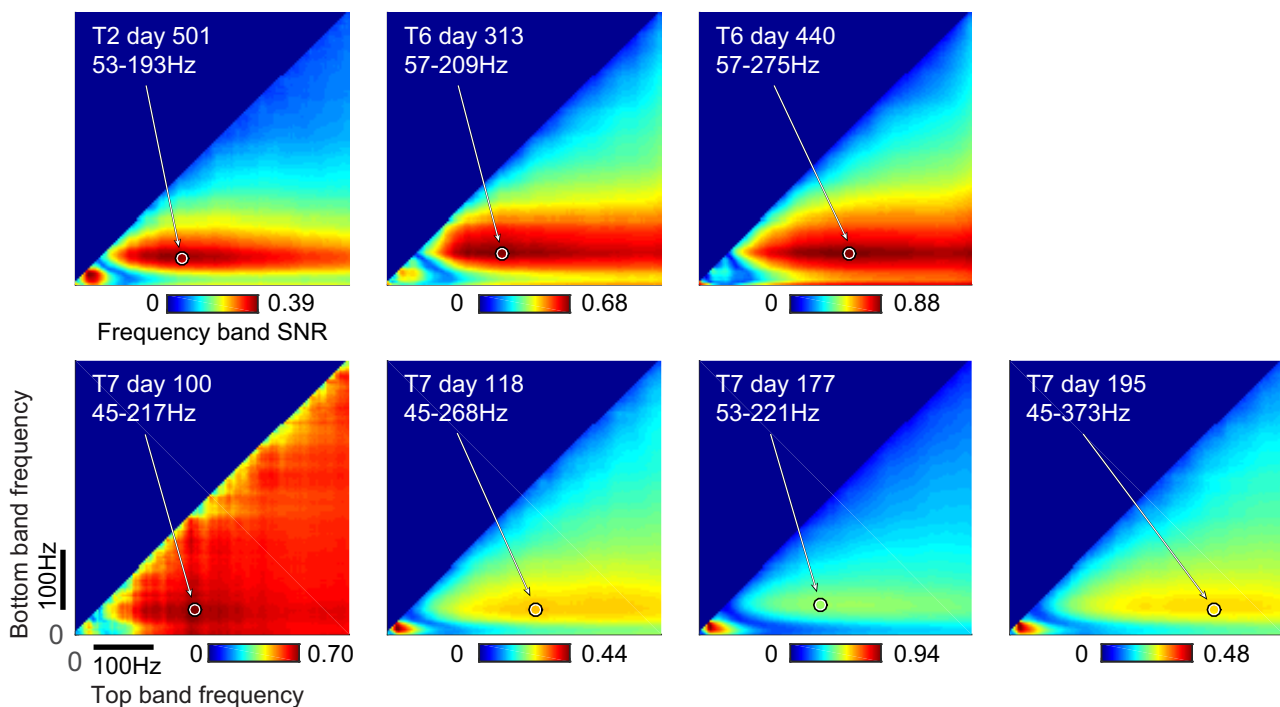


Fig. 3. Frequency band signal-to-noise ratio ( $SNR_{FB}$ ) for each session used to identify frequency bands used for cursor control. For session T7 day 100, we used a single-electrode  $SNR_{FB}$  to identify the frequency band. For all other sessions, we used an electrode-average  $SNR_{FB}$ . Black circles and arrows show the identified local maximum of  $SNR_{FB}$  above with bottom band frequency above 40 Hz. Top and bottom frequencies of the  $SNR_{FB}$  local maximum are written in white.

(termed  $|\Delta X|_{BLOCK}$ ; Fig. 2B). The confidence interval of  $|\Delta X|$  was calculated using a bootstrap procedure with 10,000 resamples (Moore et al. 2009). We also estimated the mean cursor-to-target distance in the case of no control by randomly shuffling the order in which the targets appeared (Fig. 2C). The same targets as in the corresponding test session were used and cursor position remained the same, thus keeping the cursor and target position distributions identical. The shuffling procedure was repeated 10,000 times and we calculated  $|\Delta X|$  for each repetition.  $|\Delta X|_{SHUFFLE}$  was calculated as the mean of  $|\Delta X|$  values and its confidence interval was estimated from the distribution of  $|\Delta X|$  values. Statistical significance was tested by assuming that both  $|\Delta X|_{BLOCK}$  and  $|\Delta X|_{SHUFFLE}$  followed Gaussian distributions and comparing them using the *t*-test. To account for the differences in the  $|\Delta X|_{SHUFFLE}$  between blocks, we estimated a relative improvement in control (*RIC*):

$$RIC = \frac{\langle |\Delta X| \rangle_{SHUFFLE} - \langle |\Delta X| \rangle_{BLOCK}}{\langle |\Delta X| \rangle_{SHUFFLE}}$$

The volitional control performance for the whole session (overall) was estimated by grouping all test blocks together and calculating  $|\Delta X|_{BLOCK}$ ,  $|\Delta X|_{SHUFFLE}$ , and *RIC* (see Fig. 2D for an example). When comparing performance between parts of the session, test blocks within a given part were grouped together to calculate  $|\Delta X|_{BLOCK}$ ,  $|\Delta X|_{SHUFFLE}$ , and *RIC* for that part of the session. *RIC* of 0 would indicate that the participant had no volitional HFSB-LFP control, while a positive *RIC* significantly different from 0 would indicate volitional HFSB-LFP control (see Fig. 4 for examples). Higher *RIC* indicated more accurate volitional HFSB-LFP control, while a maximum *RIC* value of 1 described cursor movements that overlapped the target during the entire block. Intermediate *RIC* values describe cursor control in which the cursor position fluctuates around the target with the size of the fluctuations inversely proportional to the *RIC* value.

To provide another, more intuitive metric of performance, we measured participants' mean normalized path to target and the mean normalized time to target. To obtain the normalized path for target *k*,  $P_k$ , the path from the moment of appearance to the moment it was acquired was divided by the edge-to-edge distance between the cursor and the target at the moment the target appeared:

$$P_k = \frac{\sum_{i=1}^N \left| |\Delta X_k|_i - |\Delta X_k|_{i-1} \right|}{|\Delta X_k|_0}$$

where *i* denotes all moments when the screen was refreshed, going from 0 (target appearance) to *N* (the moment the target was acquired).

We calculated the normalized time to target for target *k*,  $T_k$ , as the time needed to acquire the target divided by the edge-to-edge distance between the cursor and the target at the moment the target appeared:

$$T_k = \frac{^k t_N - ^k t_0}{|\Delta X_k|_0}$$

where  $^k t_0$  and  $^k t_N$  are the moments when the target appeared and was acquired, respectively. Occasionally, the target appeared close to the cursor, making the denominator small or 0, therefore making the  $T_k$  values large (or infinite) independently of participants' control. To avoid these artificially large values affecting our measure, we omitted them from calculating the statistics of the normalized time to target.

We calculated the mean normalized path and mean time to target as means of normalized paths to target and normalized times to target over all targets in one session, respectively. We calculated the distribution of the baseline mean normalized paths and mean times to target by keeping the cursor positions and shuffling the targets, as for calculation of baseline *RIC*. We randomly shuffled the target positions

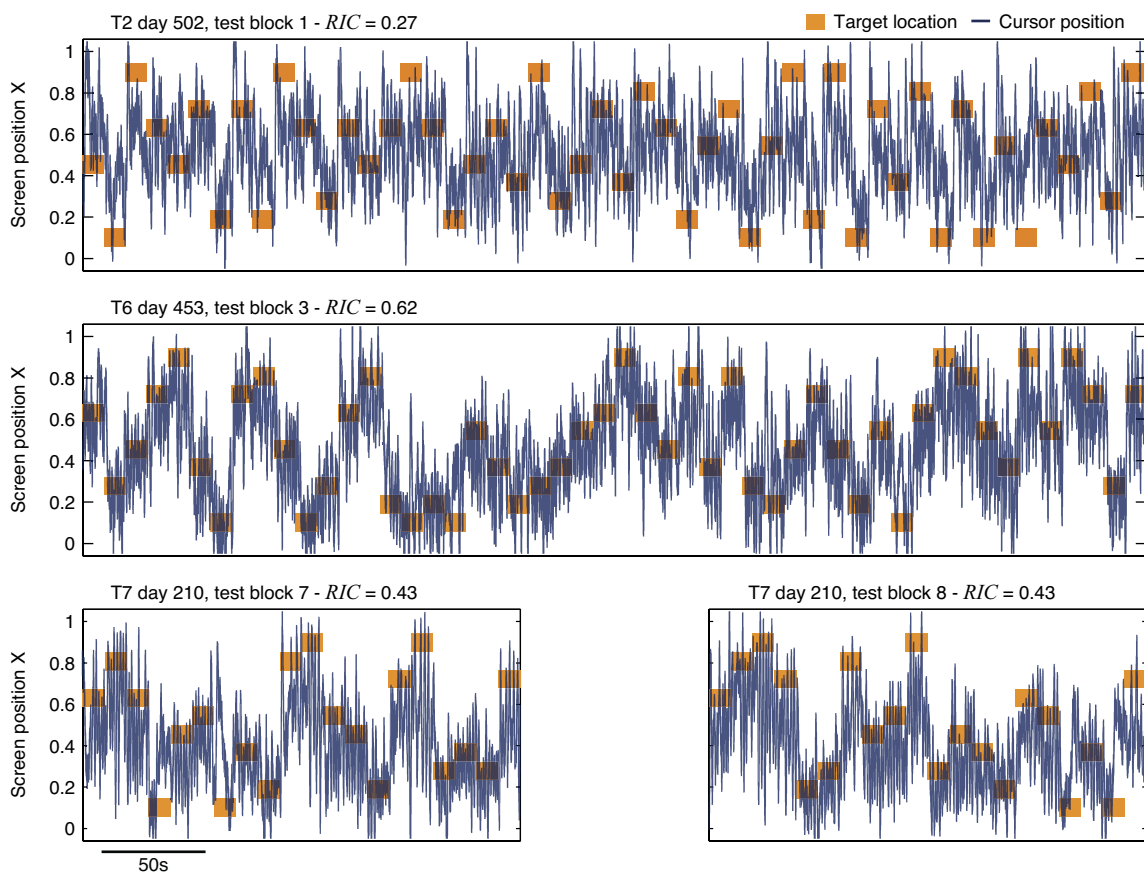


Fig. 4. Examples of blocks with targets for each of the participants in the study. In this figure, target color was changed from green to orange to improve visibility.



10,000 times and calculated the mean normalized path and mean time to target for each shuffle. Since the shuffled mean normalized path and mean time to target distributions were not Gaussian, we used the Monte Carlo method to calculate the significance of the participants' mean normalized path and mean time to target:

$$p = \frac{N_{LE} + 1}{N_{ALL} + 1}$$

where  $N_{LE}$  is the number of mean normalized paths or mean times to target calculated after shuffling the targets that are lower or equal to the participant's mean normalized path or mean time to target and  $N_{ALL} = 10,000$  is the number of random shuffles, respectively.

**Signal processing delay.** Delay between the neural activity and the cursor movements controlled by that neural activity may influence BCI performance (Cunningham et al. 2011). In our study, signal processing allowed for manipulation of the feedback delay, although at the cost of neural feature variability. By changing the delay, we investigated whether feedback delay influenced the participant's ability to volitionally control HFSB-LFPs as follows.

In our system, delay was in part caused by signal processing. During the experiment, our software used STFT to estimate spectral amplitudes of signals recorded in the last 256 or 128 ms. Since STFT gives the spectral amplitude estimates for the middle of the window, we estimated its contribution to the delay to be 128 and 64 ms for STFT windows of 256 and 128 ms, respectively. We empirically measured the contribution of the LWMA filter to the delay to be 220 and 110 ms for filter lengths of 0.8 and 0.4 s, respectively (see APPENDIX for details). Additional delay caused by the time taken to collect the neural recordings and calculate the cursor position was measured to be less than 20 ms for all sessions (length of the software iteration step) and was considered negligible. Thus, in sessions conducted with STFT window lengths of 256 and 128 ms and LWMA filter lengths of 0.8 and 0.4 s, the signal processing delay was 348 and 174 ms, hereafter referred to as long-delay and short-delay sessions, respectively.

In addition to feedback delay, changing the processing affected the feedback that participants observed. Shorter STFT window and shorter LWMA filter introduced higher frequency cursor movements. In contrast, longer STFT window and longer LWMA filter effectively filtered-out those higher frequency cursor movements.

**Identifying contributions of action potentials toward cursor control.** Recent studies showed that spiking activity of neurons in the vicinity of recording intracortical microelectrodes can contribute to LFPS (Buzsáki et al. 2012) even just above tens of Hz (Waldert et al. 2013). Our intention was to demonstrate the volitional control of a signal that does not rely on spiking activity of well-discriminated neurons, since other studies have shown that these recorded neuronal activities can be unstable (Perge et al. 2013) or deteriorate with time (Barrese et al. 2013; Dickey et al. 2009). Since the participants controlled LFPS in frequency bands that may contain contributions from spiking activity of neurons with amplitudes large enough to be detected by spike sorting, we designed an algorithm to identify whether a signal from a spiking neuron was recorded by an individual electrode. Detailed description of this algorithm is provided in the Supplemental material. Briefly, the algorithm is composed of two steps. In the first step, we use the automated spike sorting algorithm based on density grid contour clustering and subtractive waveform decomposition to identify potential spike shapes (algorithm described in details in Vargas-Irwin and Donoghue 2007). In the second step, we calculated the limiting amplitude  $a_{LIM}$  based on the distribution of the signal recorded on that electrode. Potential spike shapes with an amplitude larger than  $a_{LIM}$  are identified as neuronal spikes, while those below  $a_{LIM}$  are discarded as signal fluctuations.

For sessions in which the neuronal spikes were identified in recordings of an electrode used for LFP-based cursor control, we calculated the cursor control performance in the absence of action

potentials of the identified neuron as follows. First, the spike-sorting algorithm classified all identified threshold crossings for that session as belonging or not belonging to that neuron. An action potential response was then calculated by averaging the common average referenced wideband MEA recording from the electrode used for cursor control, triggered on the threshold crossings belonging to the identified neuron. The time epoch used for averaging was from 16.67 ms before the threshold crossing to 50 ms after the threshold crossing. We then subtracted the action potential response from the common average referenced wideband MEA recording at every threshold crossing that belonged to the identified neuron. To avoid high-frequency artifacts of the subtraction, we subtracted only the action potential response from the first to the last zero-crossing within the time epoch. The resulting signal was used to recalculate the cursor positions and the corresponding *RIC* in the absence of identified action potentials. This *RIC* was compared with the *RIC* calculated from the cursor control session. If the difference was statistically significant, the session was declared spike contaminated.

While the subtraction of average spike waveforms substantially reduces the contamination of spiking signals in LFPS, this contamination cannot be completely removed (Zanos et al. 2011).

**Mapping the topographical and spectral specificity of the volitional control signal.** To investigate the topographical specificity of the signal used for volitional control (HFSB-LFP on the electrode used for volitional control,  $el_c$ ) in the selected high-frequency band, we calculated the Pearson's linear correlation coefficient  $CC_{el}(blk)$  between this signal and HFSB-LFP on every other electrode,  $el$ , across time  $t_{blk}$  over the test block,  $blk$ .

$$CC_{el}(blk) = \frac{\text{cov}[\text{HFSB-LFP}(el, t_{blk}), \text{HFSB-LFP}(el_c, t_{blk})]}{\sigma[\text{HFSB-LFP}(el, t_{blk})]\sigma[\text{HFSB-LFP}(el_c, t_{blk})]}$$

We used the mean of  $CC_{el}(blk)$  across all test blocks in a session,  $CC_{el}$ , to see the topographical distribution of the correlation.

To investigate spectral specificity, we calculated the Pearson's linear correlation coefficient between HFSB-LFP on  $el_c$  and the mean normalized spectral band amplitudes of LFP, SB-LFP, in all other electrodes  $el$  and frequency bands (from  $f_b$  to  $f_i$ ) that did not overlap with the frequency band used for cursor control,  $CC(el, f_b, f_i, blk)$ .

$$CC(el, f_b, f_i, blk) = \frac{\text{cov}[\text{SB-LFP}(el, f_b, f_i, t_{blk}), \text{HFSB-LFP}(el_c, t_{blk})]}{\sigma[\text{SB-LFP}(el, f_b, f_i, t_{blk})]\sigma[\text{HFSB-LFP}(el_c, t_{blk})]}$$

For each participant, we used the absolute value of the mean of  $CC(el, f_b, f_i, blk)$  over all electrodes, blocks, and sessions,  $CC_{mean}(f_b, f_i)$ , to identify frequency bands that correlated or anticorrelated with the volitional control signal. We then calculated the Pearson's linear correlation coefficient between HFSB-LFP on  $el_c$  and the mean normalized spectral amplitude LFP in the identified bands for every electrode,  $el$ , across time  $t_{blk}$  over the test block,  $blk$ . This gave us the topographical distribution of correlation between the signal used for volitional control and the LFP in other bands.

## RESULTS

During the 15 cursor control sessions (T2: 1 session; T6: 5 sessions; T7: 9 sessions), participants with tetraplegia attempted to volitionally control HFSB-LFPs recorded from one MEA electrode. Controlled HFSB-LFPs were visualized as a cursor moving in the vertical dimension (up-down). Participants' volitional HFSB-LFP control was estimated through their ability to move a cursor to displayed targets, as measured by the relative improvement in control (*RIC*) with values between 0 (no volitional control) and 1 (cursor always on current target).

**Volitional control of LFPS.** Based on the *RIC* measure, all three participants were able to achieve volitional control of

cortical LFP signals and control 1D cursor movements. T2 and T6 had volitional HFSB-LFP control in all of their sessions (1 and 5 sessions, respectively), while T7 had volitional HFSB-LFP control in 5 of 9 sessions (Fig. 5A).

T2 had volitional HFSB-LFP control in all test blocks (4 of 4).

T6 had volitional HFSB-LFP control during all test blocks in all sessions (20 of 20). She often reported that she used a combination of movement imagination and attempts and sometimes reported that cursor control “felt like second nature to her.”

T7 had variable volitional HFSB-LFP control across and within days, achieving control as measured by *RIC* on 34 of 78 total blocks. In the first two sessions, he had volitional HFSB-LFP control in only 1 of 8 blocks (*T7 day 113* and *T7 day 158*). During these two sessions, T7 reported becoming less engaged with the task during long test blocks. At his request, all of his subsequent sessions were short test block sessions. In the following three sessions, T7 gained and lost volitional HFSB-LFP control during individual sessions (number of test blocks with statistically significant *RIC*: *T7 day 188*: 6 of 10; *T7 day 195*: 1 of 10; *T7 day 199*: 6 of 10). Three additional sessions

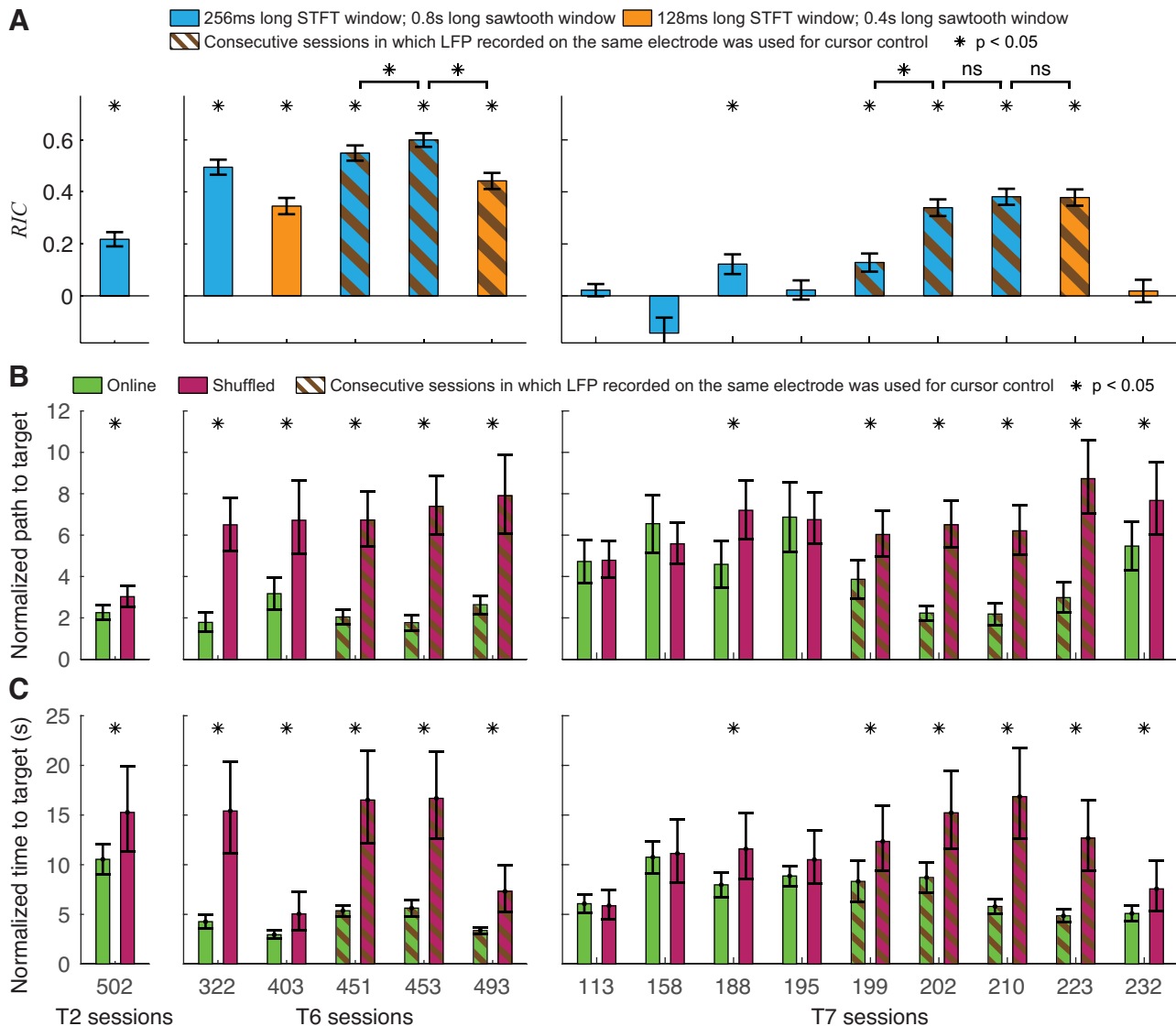


Fig. 5. Cursor control performance of participants in all completed sessions. **A**: overall relative improvement in control (*RIC*) for all completed sessions. For three participants, horizontal axis shows days after microelectrode array implantation. Most sessions evaluated cursor control using a long feedback delay and a local field potential (LFP) signal from a different electrode each day (solid blue bars). For T6 and T7, we further investigated the effect of feedback delay on volitional control by changing the signal processing parameters to switch from “long” feedback delays (bars containing blue) to “short” feedback delays (four bars containing orange). For T6 and T7, we also examined volitional LFP control when the same electrode and the same frequency band was used for cursor control across consecutive sessions (brown-striped bars). \*Statistically significant *RIC* values ( $P < 0.01$ , rank sum test). **B**: bar plot shows normalized path to target measured from testing blocks (online) and after randomly shuffling the targets in all testing blocks 10,000 times (shuffled). Bars and error bars for online condition show mean and standard errors over all targets. Bars, lower and upper error bars for shuffled condition show the median, 5th and 95th percentile over 10,000 shuffles. \*Statistically significant differences between online and shuffled conditions ( $P < 0.05$ , Monte Carlo test). **C**: bar plot shows normalized time to target measured from testing blocks (online) and after randomly shuffling the targets in all testing blocks 10,000 times (shuffled). Bars and error bars for online condition show mean and standard errors over all targets. Bars, lower, and upper error bars for shuffled condition show the mean, 5th, and 95th percentile over 10,000 shuffles. \*Statistically significant differences between online and shuffled conditions ( $P < 0.05$ , Monte Carlo test).

with short test blocks followed (*T7 day 202*, *T7 day 210*, and *T7 day 223*) where T7 had volitional HFSB-LFP control in all test blocks (30 of 30). In his last session, T7 had no volitional HFSB-LFP control in any of the test blocks (*T7 day 232*; 0 of 10).

Normalized path-to-target and normalized time-to-target measures show similar results to the *RIC* measure (Fig. 5, *B* and *C*). Both normalized path and normalized time to target were smaller for larger *RIC* values and vice-versa. For all sessions with significant *RIC*, we observed significantly smaller normalized path to target and normalized time to target compared with baseline ( $P < 0.05$ , Monte Carlo test). *Session T7 232* was the only session that showed significantly smaller normalized path to target and normalized time to target compared with baseline ( $P < 0.05$ , Monte Carlo test) but did not show significant *RIC*. Since we designed *RIC* to specifically measure the performance in the frame of the task—to acquire the target as fast as possible and keep it acquired for as long as possible—we have decided to refer to the more conservative *RIC* when considering the existence and the level of performance in our 1D cursor control task.

*Improvement of volitional LFP control through biofeedback.* During test blocks, participants received direct feedback of their neural activity and score (reward), and they were aware of the relationship between the two. This task aimed to reinforce neural activity that resulted in higher scores and, thus, to improve the volitional control of HFSB-LFPs used to control the cursor. To evaluate whether participants can improve their volitional HFSB-LFP control through prolonged use of a biofeedback paradigm, we conducted successive sessions in which participants controlled HFSB-LFPs recorded on the same electrode and in the same frequency bands (Fig. 5A). Five long-delay sessions were performed to that end (*T6 days 451* and *453*; *T7 days 199*, *202*, and *210*). For both T6 and T7, *RIC* increased significantly from the first to second sessions (*RIC* increase: T6:  $0.050 \pm 0.040$ ,  $P < 0.05$ ; T7:  $0.211 \pm 0.048$ ,  $P < 0.05$ ). For T7, who also performed a third long-delay session, *RIC* increased further in the third session (*T7 day 223*), but the increase was not significant (*RIC* increase:  $0.042 \pm 0.045$ ,  $P = 0.12$ ).

*Effect of signal processing delay on cursor control.* We conducted two feedback delay-delay sessions with both T6 and T7 (*T6 days 403* and *493*; *T7 days 223* and *232*). All other sessions were of long-delay type. One short-delay session for both T6 and T7 (*T6 day 493* and *T7 day 223*) used the HFSB-LFP from the same frequency band and the same electrode for cursor control as in the preceding successive long-delay sessions (*T6 days 451* and *453*; *T7 days 199*, *202*, and *210*). *RIC* in *T6 day 493* was significantly lower than *RIC* in *T6 day 453* (*RIC* difference:  $-0.157 \pm 0.041$ ,  $P < 0.05$ ) while *RIC* in *T7 day 223* was not significantly different from the *RIC* in *T7 day 210* (*RIC* difference:  $-0.003 \pm 0.044$ ;  $P = 0.91$ ).

For T6, *RIC* in the other short-delay session was significantly lower than *RIC* during any long-delay session ( $P < 0.05$ ), while T7 had no volitional HFSB-LFP control during the other short delay sessions (*T7 day 232*). Possible explanations for these results are presented in the DISCUSSION.

*Within-session changes of volitional LFP control.* To estimate whether volitional HFSB-LFP control changes within a session, we compared *RIC* from the first half of the session

with the *RIC* from the second half of the session (Fig. 6). Significant *RIC* increase was found in only 3 of 15 sessions (*T6 days 322* and *493*; *T7 day 188*), while none of the other sessions showed a significant decrease in *RIC* ( $P < 0.05$ ). In all other sessions, the difference was not significant. Over all sessions, first half *RIC* was not significantly different from second half *RIC* ( $P = 0.64$ , signed rank sum test).

*Cursor control contribution of action potentials of well-discriminated neurons.* On all sessions except *session T2 day 502* (14 of 15), the spike-identification algorithm did not detect any distinguishable action potentials (Fig. 7A). For *session T2 day 502*, we calculated *RIC* in the absence of identified action potentials and found that it was only 6% smaller and not statistically significantly different than the *RIC* from the cursor control session ( $P = 0.60$ , *t*-test; Fig. 7, *B* and *C*). Therefore, we considered the cursor control in all sessions unaffected by the action potentials of well-discriminated neurons.

*Topographical and spectral specificity of the volitional control signal.* We investigated the topographical specificity of the volitional control signal using the Pearson's linear correlation coefficient  $CC_{el}$  between the HFSB-LFP on electrode used for volitional control and the HFSB-LFP on all other electrodes. To determine the influence of the LWMA filter on the topographical specificity of the HFSB-LFP, we calculated the  $CC_{el}$  for three different cases: 1) without temporal filtering, 2) using 0.4-s-long LWMA filter used in the short delay sessions, and 3) using 0.8-s-long LWMA filter used in the long delay sessions. 0.4-s-long LWMA led to a substantial increase in  $CC_{el}$  across the array, while doubling the LWMA length increased  $CC_{el}$  further by a small yet significant amount (average  $CC_{el}$ : no LWMA:  $0.158 \pm 0.004$ ; 0.4 s LWMA:  $0.418 \pm 0.007$ ; 0.8 s LWMA:  $0.440 \pm 0.007$ ;  $P < 0.001$  for all pairwise comparison; Wilcoxon signed rank test). For all three signals, the areas of highest  $CC_{el}$  were located close to the electrode used for cursor control (Fig. 8A). We then investigated the relationship between  $CC_{el}$  and the distance from the electrode used for

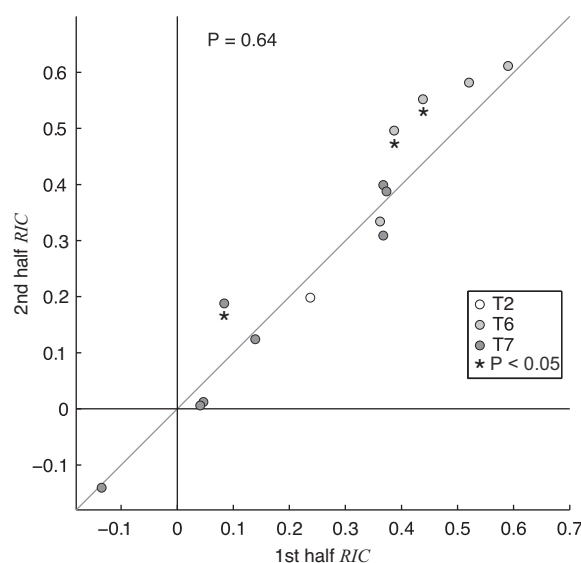


Fig. 6. Scatter plot showing relative improvement in control (*RIC*) from the 1st and 2nd halves of each session. Individual sessions where 2nd half *RIC* was significantly higher than 1st half *RIC* ( $P < 0.05$ , *t*-test) are marked with an asterisk. Over all sessions, 1st half *RIC* was not significantly different from 2nd half *RIC* ( $P = 0.64$ , signed rank sum test). T2, T6, T7, individual participants.

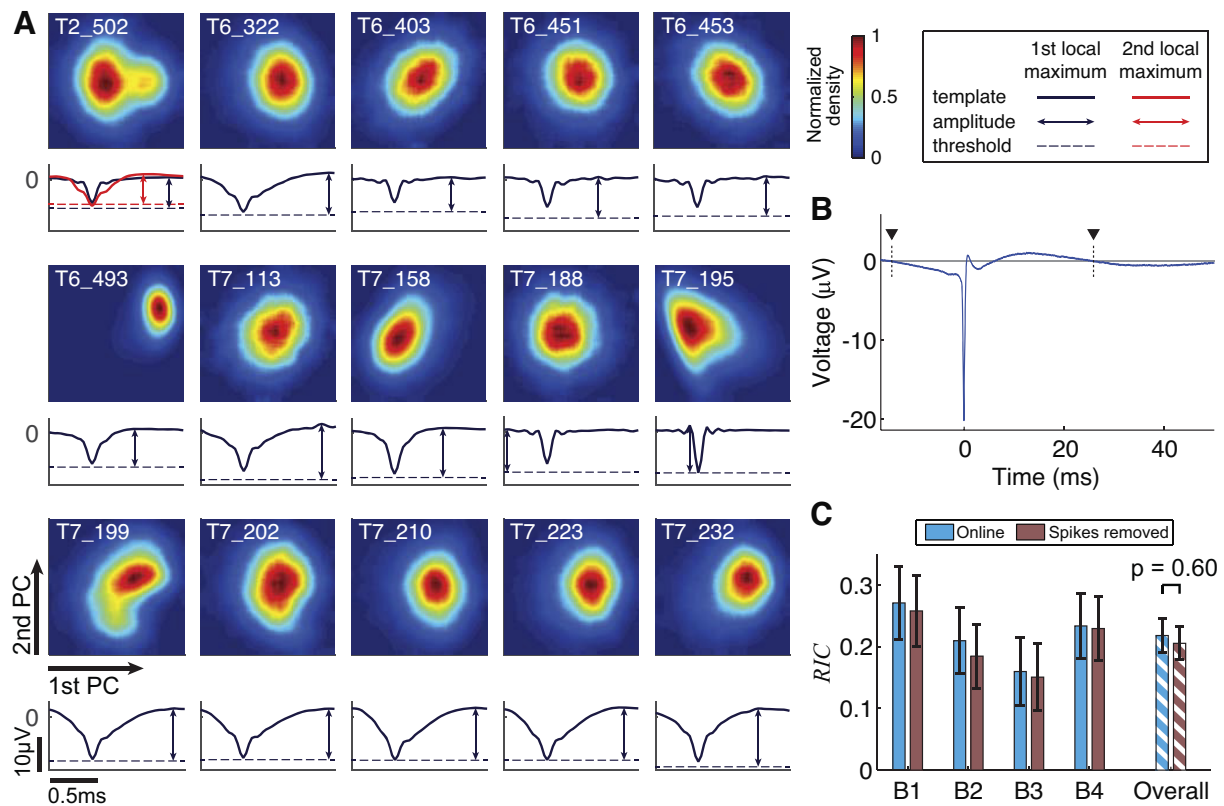


Fig. 7. Evaluating the possible contribution of action potentials of neurons in the neighborhood of the electrode used for cursor control. *A*: identification of action potentials of neurons in the neighborhood of the electrode used for cursor control. For each cursor control session, a pair of panels show the results of the neuron identification procedure. *Top* (heat maps): density of threshold crossings in the space spanned by the first two principal components (PCs). Density has been normalized to the maximum density. *Bottom*: mean of all threshold crossings contained within the 95% of local maximum density contour (full line), and the limit spike shape amplitude  $a_{LIM}$  originating from the spike shape maximum (line with arrows) and as a threshold (broken line). Out of all cursor control sessions, a single active neuron was identified for *session T2 day 502* only (first row, first column, red spike shape). *B*: cursor control contribution of actions potentials of neurons in the neighborhood of the electrode used for control in *session T2 day 502*. Mean action potential shape (blue line) and standard error of the mean (transparent blue tube, not easily seen due to small values) of the action potential identified for *session T2 day 502*. The shape from the first zero crossing (left black triangle) to the last zero crossing (right black triangle) was subtracted from the electrode recordings used for control in *session T2 day 502* to get the recordings with spikes removed. *C*: We then used the recordings with spikes removed to recalculate the cursor positions and used those to calculate the relative improvement in control (*RIC*) for each test block and overall. *RIC* calculated from signals with spikes removed was compared with the *RIC* from the cursor control session. The difference was not significant.

cursor control by measuring the mean of  $CC_{el}$  over all sessions with significant *RIC*, and then grouping them according to the distance. Without the LWMA filter,  $CC_{el}$  falls rapidly within the first 1 mm and then remains below 0.3 (Fig. 8*B*). Use of both LWMA filters systematically increases the  $CC_{el}$  for distances of up to  $\sim 2.5$  mm. For larger distances, as well as for T2 across the whole range of distances, the average increase of  $CC_{el}$  became variable, likely due to limited number of samples (Fig. 8*B*).

We then investigated spectral specificity of the volitional control signal by calculating the Pearson's linear correlation coefficient  $CC(el, f_b, f_r, blk)$  between the HFSB-LFP on electrode used for volitional control and the mean normalized spectral band amplitudes of LFP in all other electrodes and all frequency bands that did not overlap with the frequency band used for cursor control. We then used the mean of  $CC(el, f_b, f_r, blk)$  over all electrodes, blocks, and sessions for each participant,  $CC_{mean}(f_b, f_r)$ , to identify frequency bands that correlated or anticorrelated with the HFSB-LFP on electrode used for volitional control. The absolute value of  $CC_{mean}(f_b, f_r)$  revealed two frequency bands in each participant (Fig. 9). The low-frequency band correlated with the HFSB-LFP on electrode

used for volitional control (T2: 0–2 Hz,  $CC_{mean} = 0.015$ ; T6: 0–21 Hz,  $CC_{mean} = 0.108$ ; T7: 0–6 Hz,  $CC_{mean} = 0.022$ ). The intermediate-frequency band anticorrelated with the HFSB-LFP on electrode used for volitional control (T2: 21–19 Hz,  $CC_{mean} = -0.092$ ; T6: 25–33 Hz,  $CC_{mean} = -0.060$ ; T7: 18–25 Hz,  $CC_{mean} = -0.085$ ).

We then examined the topographical distribution of the correlation between the HFSB-LFP of the electrode used for cursor control and the mean normalized amplitude in the identified low and intermediate spectral bands, LFSB-LFP and IFSB-LFP, for all electrodes of the microelectrode array (Figs. 10 and 11). The topographical distribution of the mean correlation between HFSB-LFP and LFSB-LFP in the selected bands and across all blocks,  $LFSB-CC_{el}$ , showed higher correlation near the electrodes used for cursor control (Fig. 10*A*). Nonetheless, the values were smaller compared with  $CC_{el}$  (below 0.15) and settled into a constant value already after the distance of  $\sim 1$  mm (Fig. 10*B*).

Unlike for the other two bands, the topographical distribution of the mean absolute correlation across all blocks in the intermediate-frequency band,  $IFSB-CC_{el}$ , consistently showed lower values at and around the electrode used for cursor control

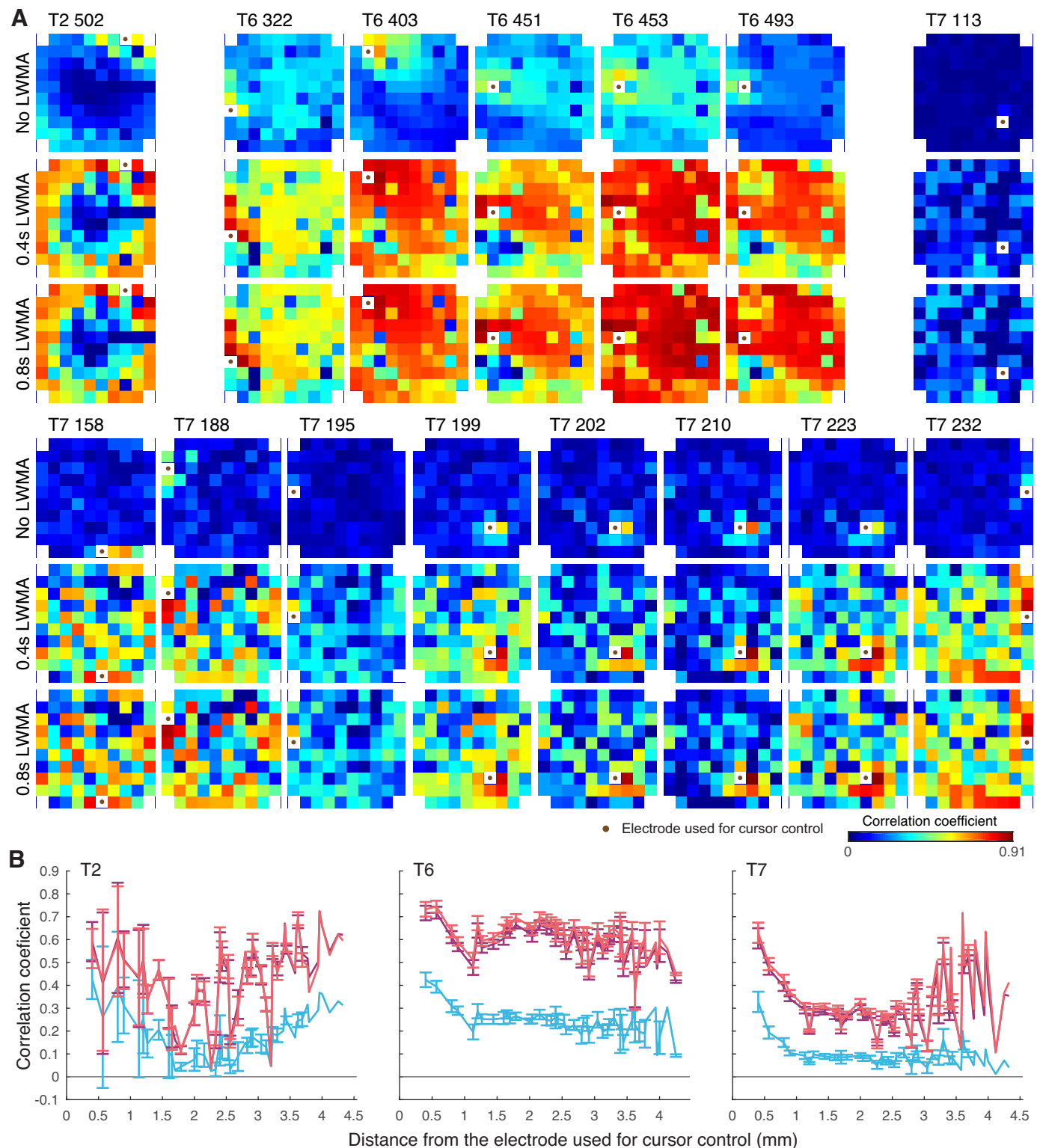


Fig. 8. Correlation between the local field potential (LFP) used for volitional control [high-frequency selected band of LFPs (HFSB-LFP) on the electrode used for volitional control] and the HFSB-LFP on other electrodes of the intracortical array without filtering the HFSB-LFP using the linear weighted moving average [no linear weighted moving average (LWMA)], filtered using 0.4-s-long LWMA (0.4 s LWMA), and filtered using 0.8-s-long LWMA (0.8 s LWMA). *A*: color plots show the Pearson's correlation coefficient between the HFSB-LFP on the electrode used for control and all other electrodes for the frequency band used for control ( $CC_{ij}$ ) calculated over all test blocks in the session. For each session, *top*, *middle*, and *bottom* rows show the correlation obtained without filtering the HFSB-LFP, when filtering the HFSB-LFP using 0.4 s LWMA, and when filtering the HFSB-LFP using 0.8 s LWMA. A brown dot denotes the electrode used for cursor control. *B*: plots show  $CC_{ij}$  for different distances from the electrode used for cursor control for each participant (T2, *left*; T6, *middle*; T7, *right*) for three temporal filters of the HFSB-LFP (blue: no LWMA; magenta: 0.4 s LWMA; red: 0.8 s LWMA).

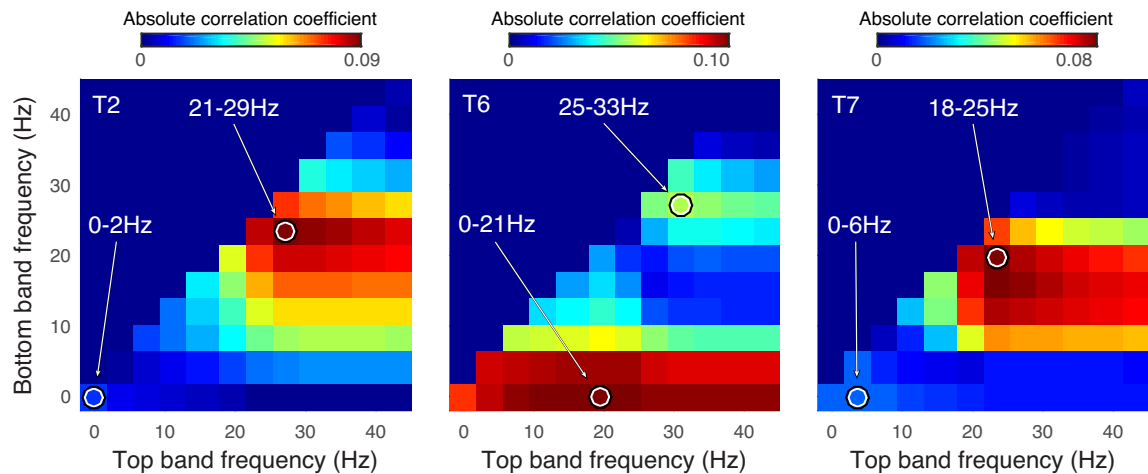


Fig. 9. Identification of frequency bands that correlated or anticorrelated with the neural control signal. Color plots show absolute value of the mean of electrode- and frequency band-dependent Pearson's linear correlation coefficient  $CC(el,fb,ft,blk)$  across all blocks, electrodes, and sessions for each participant (T2, *left*; T6, *middle*; T7, *right*). The analysis uncovered one low-frequency band that correlated with the control signal and one intermediate-frequency band that anticorrelated with the control signal.

(Fig. 11A). In fact,  $IFSB-CC_{el}$  was consistently close to 0 at the electrode used for cursor control and then became increasingly negative as the distance from the electrode used for cursor control increased, thus indicating larger anticorrelation (Fig. 11B). The anticorrelation increase settled within the distance of  $\sim 1$  mm to a small absolute value (above  $-0.15$ ) when compared with  $CC_{el}$ .

## DISCUSSION

Here, we demonstrated that people with tetraplegia can volitionally control spectral LFP amplitudes in the HFSB (a subband of the 40–400 Hz frequency band) recorded from one electrode using a biofeedback BCI. Volitional HFSB-LFP control was achieved in the majority of cursor control sessions conducted with each study participant: 1 of 1 conducted with participant T2, 5 of 5 with T6 and 5 of 9 with T7. Our results also imply that volitional HFSB-LFP control can improve when using a biofeedback BCI over consecutive sessions conducted several days apart. When participants T6 and T7 volitionally controlled HFSB-LFPs from the same electrode and in the same frequency band that was used in the previous cursor control session 2 and 3 days earlier, respectively, their control increased significantly (tested only once in each participant). For T7, conducting an additional cursor control session 8 days after the second one, where the HFSB-LFP from the same electrode and in the same frequency band was used again, led to a small but not statistically significant increase in performance. This implies that the initial  $RIC$  increase observed between the first and the second session can be retained for more than a week.

We hypothesized that use of a relatively movement-information-poor signal (LFPs from a channel lacking identifiable spiking activity) from a single point in motor cortex would be sufficient to permit a cursor to hover over up to 10 distinct vertical locations on a screen by people with tetraplegia and that a biofeedback paradigm could be used to improve this LFP-based cursor control. The task, while simple compared with the multidimensional reach-and-grasp and point-and-click typing tasks previously demonstrated with MEAs (Ajiboye et al. 2017; Bacher et al. 2015; Bouton et al. 2016; Collinger et al.

2013; Gilja et al. 2015; Hochberg et al. 2012; Jarosiewicz et al. 2015; Pandarinath et al. 2017; Wodlinger et al. 2015), is still considerably more difficult than the binary “upper target” versus “not upper target” field potential tasks used in classic electroencephalography sensory-motor rhythm modulation tasks (Pfurtscheller et al. 2003; Wolpaw et al. 1991; Wolpaw and Wolpaw 2012). Not unexpectedly, the absolute performance of these single-electrode, single-LFP-band tasks was not qualitatively “good”; the cursor oscillated around the targets that covered  $\sim 10\%$  of screen height with varying amplitudes. Nevertheless, the repeatedly found statistically significant improvements in this control over time speaks well toward integrating components of such LFP-based control, particularly as it may be available from multiple electrodes on the same MEA, toward ever-better hybrid neural decoders that could be useful to people with tetraplegia.

In addition to the cursor and a target, the participants were also presented with  $\sim 10$ -s history of the target movements and a numerical score, which were directly or indirectly derived from their volitionally controlled HFSB-LFPs. Therefore, these two additional sources of biofeedback may have influenced the participants' volitional control. While we introduced these biofeedback components to further encourage the participants and make their task easier, these components may have also been detrimental, for example due to splitting their attention. Additional research is needed to reach optimal biofeedback paradigm designs.

*Absence of within-session improvement in volitional control.* While volitional HFSB-LFP control did improve significantly from the beginning to end of the study within some T6 and T7 sessions, we did not consistently observe within-session improvement. Considering data from all sessions, we must conclude that volitional HFSB-LFP control did not change significantly across the test blocks within a cursor control session. As each session progressed, changes in participant concentration, arousal, attention, fatigue, engagement, or strategy could have impaired their potential to achieve and improve neural control. For example, T7 self-reported that it was sometimes difficult to remain engaged across long blocks, due in part to the relatively uninteresting control task. After the introduction

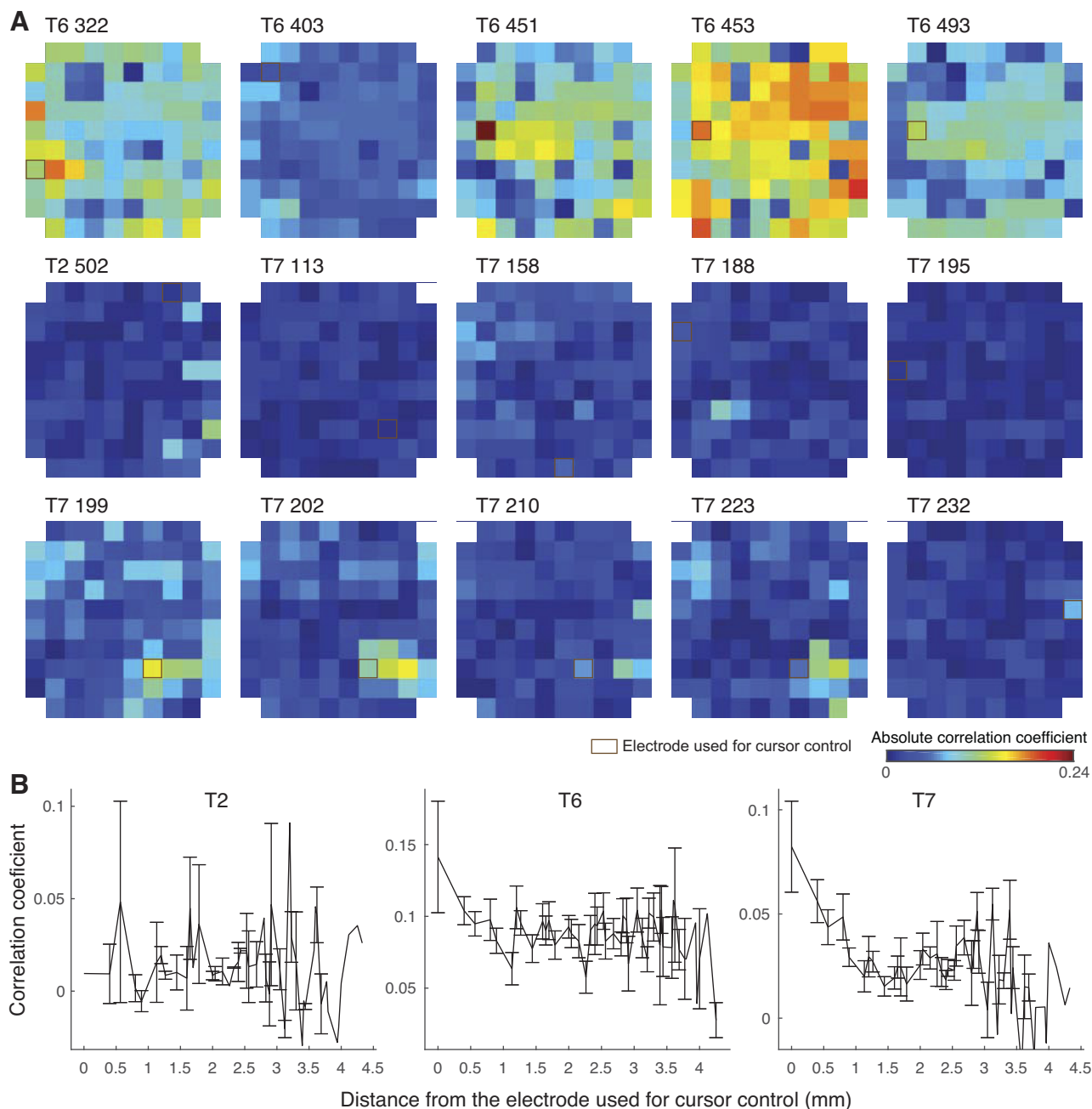


Fig. 10. Correlation between the local field potential (LFP) used for volitional control [high-frequency selected band of LFPs (HFSB-LFP) on the electrode used for volition control] and low-frequency selected band (LFSB-LFP) identified through the correlation analysis (Fig. 9). *A*: color plots show the mean absolute value of the Pearson's correlation coefficient between the HFSB-LFP on the electrode used for control and LFSB-LFP on all electrodes of the microelectrode array calculated over all the test blocks in the session,  $LFSB-CC_{el}$ . A brown square shows the electrode used for control. *B*: plots show  $LFSB-CC_{el}$  for different distances from the electrode used for cursor control for each participant (T2, left; T6, middle; T7, right).

of shorter duration blocks for T7, his performance improved to become significantly different from chance, suggesting that performance in this task, and presumably improvement, could be sensitive to degree of attention or arousal. Recent studies have shown that people with tetraplegia can use a hybrid spike and LFP-based biomimetic BCI to achieve robust two-dimensional control of the computer cursor (Gilja et al. 2015; Pandarinath et al. 2017). There, participants gained the cursor control by attempting natural movements, a strategy that may require a low amount of concentration and, thus, slower accumulation of fatigue. In contrast, biofeedback-driven control of

LFPs, where participants are not directly instructed to use any habituated context for control, but to explore and create their own context, may require higher concentration levels that may be difficult to maintain over time. It is also possible that any of these factors might have directly affected or modified LFPs throughout sessions, leading to variability in control that may have masked potential control improvements. Together, this array of possibilities motivates further understanding of the factors that influence characteristics of human LFP signals.

Another possibility is that biofeedback-based improvement in volitional LFP control occurred primarily during initial

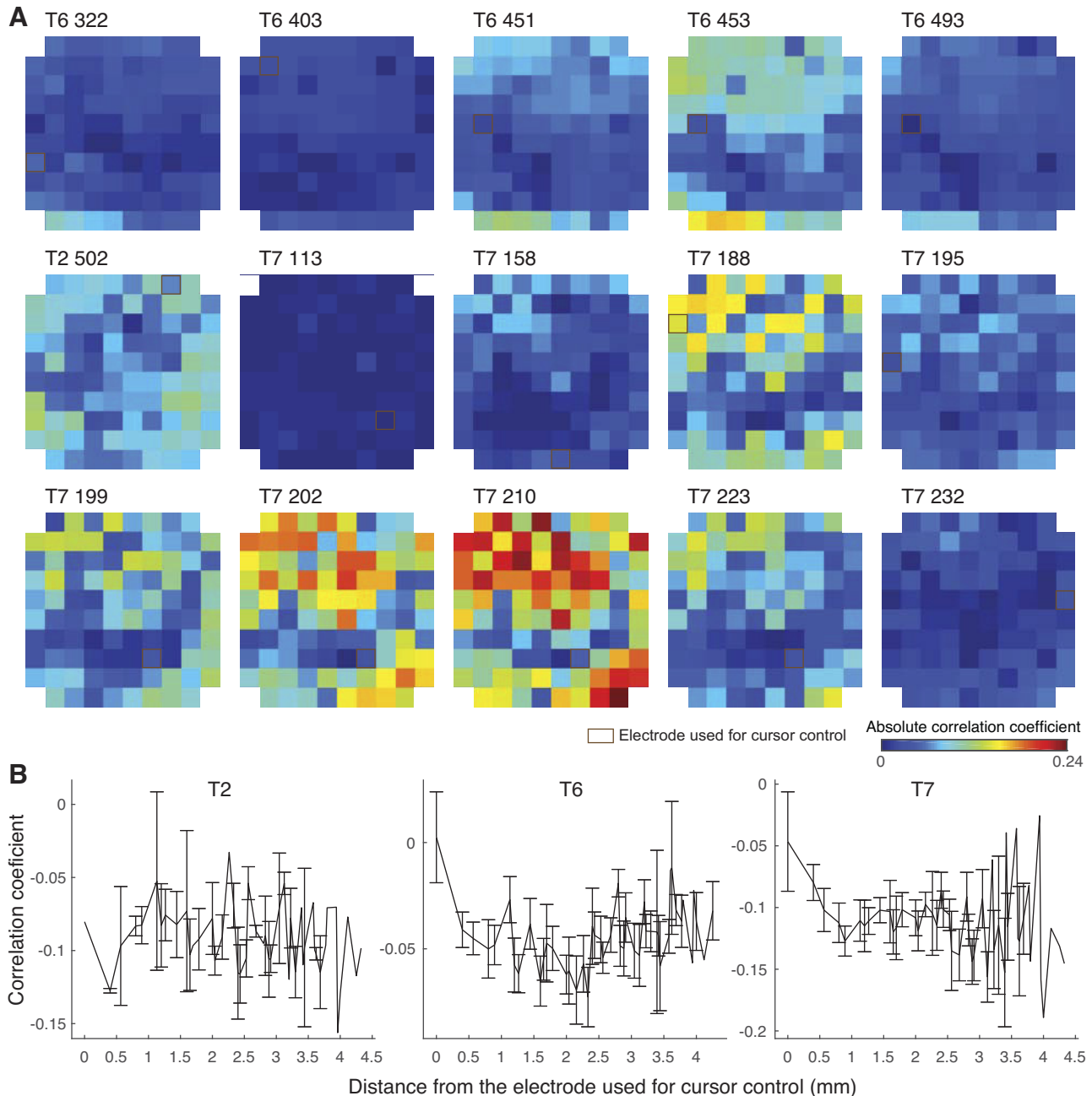


Fig. 11. Correlation between the local field potential (LFP) used for volitional control [high-frequency selected band of LFPs (HFSB-LFP) on the electrode used for volition control] and intermediate-frequency selected band (IFSB-LFP) identified through the correlation analysis (Fig. 9). *A*: color plots show the mean absolute value of the Pearson's correlation coefficient between the HFSB-LFP on the electrode used for control and IFSB-LFP on all electrodes of the microelectrode array calculated over all the test blocks in the session,  $IFSB-CC_{el}$ . A brown square shows the electrode used for control. *B*: plots show  $IFSB-CC_{el}$  for different distances from the electrode used for cursor control for each participant (T2, left; T6, middle; T7, right).

exploration blocks in which the participants had unconstrained freedom to explore different ways to improve cursor control. However, since participants' goals were not cued and their intentions were unknown to us, this "unsupervised" performance could not be quantified. In contrast, participants' freedom to explore may have been constrained during the test block by the requirement to exploit their current level of control to earn points. In some of the sessions, the participants may have started the test blocks with the maximum control that could be achieved by the used HFSB-LFP signal, thus preventing further improvements. Finally, it is likely that task param-

eters in this unique investigation of human control of LFPs were not optimal to induce improvement in LFP control. Factors to be considered include duration of and interval between blocks, total task duration, and whether a minimum performance level promotes acquisition of volitional control of these neural signals.

*Cross-session improvement in volitional control.* We observed increases in the volitional HFSB-LFP control, as measured by  $RIC$ , in consecutive cursor control sessions during which participants T6 and T7 controlled LFPs recorded from the same electrode and in the same frequency band (tested only



once in each participant). While participants may have consolidated volitional HFSB-LFP control skills gained in the previous session, they also had an opportunity to further explore control during the exploration blocks in the second session. Since control was better during the second session both times it was measured, participants found the task easier to perform and may have found it easier to stay engaged with the task as a result. With T7, we conducted a third consecutive cursor control session in which HFSB-LFP recorded from the same electrode and in the same frequency band was used for cursor control. Compared with the second session, volitional HFSB-LFP control did not improve significantly. While T7 may have reached maximum volitional control during the second session, the lack of improvement may be explained by a gap of 8 days between the second and the third sessions. T7 may have partially forgotten some of the nuances of control and had to spend part of the exploration blocks relearning them, instead of focusing on further control improvements. To maximize the improvement of volitional HFSB-LFP control by using biofeedback paradigms, it may be desirable to conduct sessions on consecutive days. Further research is needed to investigate optimal session schedules.

We studied the continued improvement of HFSB-LFP control up to the span of 24 days in total (from *T7 day 199* to *T7 day 223*). While this time span is certainly short compared with a desired lifetime of assistive devices of several years, the currently dominant strategy of daily recalibrating intracortical brain-computer interfaces to maintain performance (Ajiboye et al. 2017; Bacher et al. 2015; Collinger et al. 2013; Gilja et al. 2015; Hochberg et al. 2006, 2012; Kim et al. 2008; Pandarinath et al. 2017; Wodlinger et al. 2015) make such span relevant for the current BCI designs. Further studies are needed to investigate the longevity of volitional HFSB-LFP control gains through biofeedback.

Our approach to investigate the gains in volitional HFSB-LFP control relied of the stationarity of HFSB-LFP modulations over time, including the property that HFSB retain the same relation to participants' volitional attempts to modulate it over weeks. While we did not directly control for this property, our approach to derive HFSBs using the same movement instructions identified similar frequency bands (T6: 56.64–208.98 Hz and 56.64–277.34 Hz; T7: 52.73–220.70 Hz and 44.92–373.05 Hz). The signal-to-noise ratio (SNR) function used to identify HFSBs changed only by small amount when changing the top frequency of the HFSBs, which exhibited the largest changes over time. This indicates that HFSBs changes are partially an outcome of noisy SNR estimates resulting from limited movement attempt repetitions or inability of participants to stereotypically repeat the movement attempts within session and between sessions that were 127 and 18 days apart, respectively. Indeed, our recent study found little or no change between maximum SNR high-frequency bands of LFP responses to movement attempts of people with tetraplegia. In that study, participants attempted the same movement in five sessions spread across up to 42 days (Milekovic et al. 2018), indicating that practice and, consequently, more stereotypical movement attempts stabilize the HFSB.

*Effect of feedback delay on volitional LFP control.* Oscillations of cursor position during initial long-delay sessions raised the possibility that, due to delay caused by our signal processing, participants experienced a feedback delay and therefore

regularly overcorrected their HFSB-LFP modulations, which may have led to reduced control. We hypothesized that if this were a dominant effect, reducing signal processing delay would reduce these corrections and, thus, lead to improved control. To test this, we ran two short-delay sessions with both of T6 and T7. Instead of observing a performance increase, we found that volitional HFSB-LFP control either decreased (T6) or remained unchanged (T7). While signal processing delay and resulting participants' corrections may have an effect on the volitional HFSB-LFP control, we conclude that its influence was not dominant in this study. Improvement in control gained by changing signal processing from long delay to short delay, if any, may have been compensated for or outweighed by control decrease due to 1) less precise estimates of the spectral LFP amplitudes due to shorter STFT windows and 2) the presence of HFSB-LFP modulations in higher frequencies that would have otherwise been filtered out by LWMA filter of longer length. Limited number of experimental sessions prevent us from reaching more detailed conclusions on the effects of feedback delay and signal processing approaches on the ability of people to volitionally control their LFPS. Further research is needed to investigate optimal tradeoff between signal-processing delay and low-pass filtering of spectral LFP amplitudes that may lead to improvements in volitional HFSB-LFP control.

One short-delay session for T6 and T7 each used the LFP from the same electrode and in a similar frequency band for cursor control, as in the previous session. For T6, volitional HFSB-LFP control dropped significantly when compared with the previous session, while the difference for T7 was not significant. However, the intersession interval between those two session pairs (40 days for T6 and 13 days for T7) was longer than between the preceding long-delay sessions that used the same LFP signal for cursor control (2 days for T6 and up to 8 days for T7). Since the volitional HFSB-LFP control decline was observed only at long intersession intervals (>13 days), ability to volitionally control the LFPS with an unchanging cognitive strategy may decrease with time. However, additional time points from more participants would be necessary to answer this question.

*Potential for volitional control of multiple individual electrodes.* We investigated volitional control of a single-electrode LFP as a first step toward independent volitional control of multiple single-electrode LFPS to enable users with control of multiple degrees of freedom. However, independent volitional control of multiple single-electrode LFPS may only be possible if the used signals are specific to that electrode or its neighborhood. In our case, the neighborhood would have to be smaller than the cortical area covered by the Blackrock electrode array. Our analysis revealed that the LFP signal used for volitional control—the single-electrode HFSB-LFP filtered by a low-pass LWMA filter—is correlated with low-pass filtered HFSB-LFP on many electrodes across the microelectrode array. While the correlation was consistently higher with LFPS from electrodes near the electrode used for volitional control (1-mm neighborhood), it remained substantial even for larger distances. Nonetheless, sets of electrodes with a smaller correlation were available, indicating that our participants could have gained volitional control of multiple low-pass filtered single-electrode HFSB-LFPs recorded by a single microelectrode array. Correlation coefficients between unfiltered

HFSB-LFPs were substantially lower and, beyond the 1-mm neighborhood of the electrode used for volitional control, settled to a constant low value. This result indicates that the higher frequency components of the HFSB-LFP, removed by applying the LWMA low-pass filter, are more topographically specific. Therefore, we propose two strategies to obtain independent volitional control of multiple electrodes on the  $3.6 \times 3.6$  mm cortical area covered by a 96-electrode microelectrode array. The topographical correlation analysis employed here (Fig. 8) may reveal subsets of electrodes that are not highly correlated with the low-pass filtered HFSB-LFP of the first electrode the participant volitionally controls. The participant can then gain volitional control of a low-pass filtered HFSB-LFP of one of the electrodes from this subset with the expectation that this second volitionally controlled signal will remain uncorrelated with the first. This strategy can then be used to select the next single-electrode low-pass filtered HFSB-LFP for volitional control, until all available mutually uncorrelated electrode regions have been exhausted. Alternatively, removing the low-pass filter or increasing its attenuation frequency will retain the more localized component of the HFSB-LFP, thus increasing the number of electrodes with mutually uncorrelated signals. However, our participants had difficulties controlling the HFSB-LFP without a low-pass filter. Therefore, this strategy may come with a tradeoff: learning volitional control of each single-electrode neural signal may be more difficult and/or time consuming but may result in more topographically specific volitionally controlled signal. This, in turn, may enable volitional control of more numerous independent signals from the same set of electrodes. Further studies are needed to explore the efficacy of these strategies.

Potentially, independent volitional control of multiple signals may also be established using LFPs recorded on the same electrode but in different frequency bands. However, such spectral-band LFP signals would have to modulate synchronously and not be highly correlated or anticorrelated with the other already used volitional control signal. Prior studies have identified low- and intermediate-frequency LFP bands to exhibit coherent informative modulations (Milekovic et al. 2015, 2018; Mollazadeh et al. 2011; Rickert et al. 2005). The exact frequency bands vary between subjects, but are typically in the 0–10 Hz and 10–40 Hz range, respectively. LFP signals in these frequency bands may, therefore, be used to gain further independent volitionally controlled signals. However, this may only be possible if the LFPs in those bands are not correlated with the other, already-used signal. Our analysis showed that low-frequency LFP is only weakly correlated with the high-frequency LFP signal on the electrode used for control. Furthermore, the correlation is higher within the 1-mm neighborhood of the electrode used for control. Beyond 1 mm, the correlation settles into a constant small value. Intermediate-frequency LFP showed weak anticorrelation with the high-frequency LFP signal on the electrode used for control across the whole array. The anticorrelation was lower at the electrode used for control but was largely independent of the distance for all other electrodes. This result indicates that independent volitional control of an additional signal may also be achieved using LFPs in other frequency bands.

Nonetheless, other relations between the volitionally controlled single-electrode HFSB-LFP and the LFPs in other frequency bands that we have not revealed by our analysis

may exist. For example, phase of the low-frequency LFPs may be coupled to the HFSB-LFP across a set of electrodes, which could impede the attempts to gain independent control of HFSB-LFPs from two or more electrodes of that electrode set, or gain independent control of that low-frequency LFP and the HFSB-LFP on one of the electrodes of that electrode set. Such coupling may also limit the rate of change of the LFP signals the participants are trying to control. Further studies exploring volitional control of multiple LFP signals in different frequency bands are needed to reveal their potential for enabling volitional control of multiple interface controls.

*Relevance for clinical applications.* In this study, we show that people with paralysis can gain volitional control of LFPs as recorded from a single point in motor cortex and that their control can improve through biofeedback conducted over consecutive sessions a few days apart. Thus, the data provide a proof of concept of an LFP-based BCI for people with tetraplegia achieved using a biofeedback paradigm. Our results confirm previous results in which nonhuman primates gained volitional control of LFPs (Nishimura et al. 2013) and substantially improved their control by using a biofeedback paradigm over successive days (Engelhard et al. 2013). Our results also indicate that improvement in volitional LFP control can be retained for at least a week. Since the full potential of the biofeedback approach can be achieved only if improvements in control are retained, this is an important step toward its use in clinical applications.

Together with prior biofeedback paradigm studies in nonhuman primates (Engelhard et al. 2013; Ganguly and Carmena 2009, 2010; Moritz and Fetz 2011; Moritz et al. 2008; Nishimura et al. 2013), our findings indicate that a “biofeedback approach,” in which users gain volitional control of neural signals used for BCI control and then improve their control through biofeedback, may lead to improvements in BCI performance. The biofeedback approach, however, may be limited by three factors: 1) the ability of a BCI user to gain and improve volitional control of neural activity in the selected frequency range; 2) the ability of implanted devices to reliably record neural signals of interest as used for BCI control; and 3) the number of independent control signals embedded in recorded neural signals compared with the number of degrees of freedom needed to operate a sophisticated prosthetic device. While our study addresses some of the limitations under point 1), to further demonstrate the clinical usability of the LFP-based biofeedback approach, limitations under points 2) and 3) have to be addressed.

Nonetheless, a recent study in nonhuman primates demonstrated that intracortical LFPs can be recorded reliably for over 12 mo (Flint et al. 2013). Our recent study demonstrated that LFP modulation across low- (0–5 Hz), intermediate- (14–41 Hz), and high- (53–283 Hz) frequency bands of LFP in response to movement attempts of people with tetraplegia, two of which where the participants of this study (T2 and T6), can be stable over several months (Milekovic et al. 2018). These studies show that reliable long-term recordings of LFP signals in people is possible.

Other studies have used intracortically recorded LFPs to achieve BCI control in people with paralysis. Paralyzed participants used a communication BCI controlled by a mixture of multiunit spike and LFP features to write six words per minute

(Gilja et al. 2015). An individual with locked-in syndrome due to a brain stem stroke used a communication BCI based only on LFPS recorded using neurotrophic electrodes to write sentences (Kennedy et al. 2000, 2004). Recently, our group showed that an individual with ALS and an individual with locked-in syndrome due to brain stem stroke can use an LFP-based communication BCI to write messages and send email without recalibration over several months (Milekovic et al. 2018). This study builds on those studies by exploring the potential of biofeedback as a method to enhance the performance of LFP-based BCIs.

While our results show that people can learn to volitionally control LFPS recorded from just one MEA electrode, the same approach applied over different MEA electrodes could potentially be used to provide control of different independent degrees of freedom enabling multidimensional BCI control, such as control of a point-and-click computer cursor. Furthermore, the biofeedback approach could be used to augment methods that enable complex BCI control, e.g., control of a BCI-driven prosthetic arm or control of hand muscles in a person with paralysis through a functional electrical stimulation (FES) device. To understand the limits of this approach, it is necessary to investigate the extent to which users can volitionally independently control LFPS recorded on multiple electrodes. Nevertheless, this study provides additional support for the investigation and use of intracortically recorded LFPS and biofeedback paradigms in ongoing BCI development.

It should be noted that all the participants of this study had prior experience with BCI paradigms. Each participant was exposed to different BCI paradigms and their exposure varied both in frequency and the amount. This exposure may have contributed to the ease of acquisition of volitional control and their subsequent gains of volition control over several days in sessions that used the same HFSB-LFP signal for cursor control. Further detailed studies are needed to investigate how BCI experience affects the speed of acquisition of volitional control of neural signals.

*Comparison to biofeedback BCIs based on other neural signal modalities.* Other signal modalities studies have used BCI control (Birbaumer et al. 2009; Wang et al. 2010; Weiskopf 2012). Human participants learned to volitionally up or downregulate functional magnetic resonance imaging (fMRI) signals through biofeedback (Caria et al. 2007, 2010; Weiskopf et al. 2003, 2004). Healthy participants and people with paralysis learned to modulate EEG activity when provided direct feedback of their neural signals, and they used the learned modulations for BCI control (Birbaumer et al. 1999; Heinrich et al. 2007; Kübler et al. 1999; Leins et al. 2007; McFarland et al. 2005; Nijboer et al. 2008; Rockstroh et al. 1990). Magnetoencephalography and electrocorticography have also been used to provide participants with volitional control of their neural signal through biofeedback BCIs (Jerbi et al. 2009; Mellinger et al. 2007; Schalk et al. 2008). The majority of these studies focused on demonstrating a proof of concept that biofeedback can be used to generate volitional control of the signal by the users. Others used a trial-based design where performance was measured by a number of correctly acquired targets (Mellinger et al. 2007; Schalk et al. 2008). We have built on these experiences to develop a more complex task that would allow us to measure the level of volitional control participants exhibit over the used signal. Due to differences in

the task designs, it is difficult to estimate which of the studies demonstrated superior control. Further studies are therefore needed to establish the utility of different modalities to achieve BCI control through biofeedback.

Although biomimetic and biofeedback BCIs are distinct (as described above), most BCIs where the decoder has been calibrated using the biomimetic approach contain some aspects of the biofeedback approach. Subjects observe the movements of the effector, and this leads to the changes of the neural activity and control strategies upon which the BCI is based to improve the control (Hwang et al. 2013; Jarosiewicz et al. 2008; Taylor et al. 2002). In this study, we investigated the extent to which 1D cursor control can be achieved and improved through biofeedback with an individual LFP channel, in part as a first step toward using multiple volitionally controlled individual LFP channels. The cursor position was directly related to the neural activity recorded from this single LFP channel. All the processing that translated neural activity from that neural signal into cursor position were based only on its statistics. Therefore, we aimed to evaluate the “pure” biofeedback approach using intracortically recorded LFPS while demonstrating some ability for LFP biofeedback to be learned. Further research is needed to verify whether such strategies could compete with today’s dominant biomimetic approach for decoder calibration.

## APPENDIX

*Determining the electrodes and frequency bands used for cursor control.* Each session was composed of three blocks lasting about three and a half minutes each. During each block, the computer screen in front of the participant presented 17 visual cues. The participants were asked to react to the visual cues by performing predetermined actions (Table 4). We defined action-relevant epochs as time from the visual cue to 1.5 s after the cue. The remainder of the time was defined as baseline epoch  $T_{BASELINE}$ .

Wideband MEA recordings were first down sampled to 1 kHz with the same procedure as described in the *Preprocessing of neural signals* section. We then used STFT with a window length of 256 ms and a Hamming window to calculate spectral amplitudes  $a(el, f, t)$ , where  $el$  is the electrode signal was recorded from,  $f$  is the frequency bin, and  $t$  is time. Baseline  $a$  was calculated by applying STFT every 500 ms during the baseline epoch.  $a$  calculated from windows overlapping the action-relevant epochs were not considered as baseline. Baseline  $a$  were used to determine the mean baseline amplitude over time,  $\mu_{BASELINE}(el, f)$ .

$$\mu_{BASELINE}(el, f) = E[a(el, f, t)] \quad t \in T_{BASELINE}$$

where  $E$  is the expectation operator. Action  $a$  was calculated during the action-relevant epochs, starting from centering the window on 128 ms after the cue, moving the window in steps of 62 ms with the last window centered on 1,368 ms after the cue. We then calculated band mean normalized amplitudes (BMNA) for each possible frequency band.

$$BMNA(el, f_B, f_T, t_E, n) = \frac{1}{f_T - f_B + 1} \sum_{f=f_B}^{f_T} \frac{a(el, f, t_E, n)}{\mu_{BASELINE}(el, f)}$$

where  $f_B$  and  $f_T$  are the top and bottom frequency bins of the frequency band, respectively;  $t_E$  is the time in respect to the cue; and  $n$  is the cue number. We then calculated the SNR (Milekovic et al. 2012) for each electrode, frequency band, and time in respect to the cue.

$$\begin{aligned}\mu_{ACTION}(el, f_B, f_T, t_E) &= E[BMNA(el, f_B, f_T, t_E, n)] \\ \sigma_{ACTION}(el, f_B, f_T, t_E) &= std[BMNA(el, f_B, f_T, t_E, n), n] \\ \sigma_{BASELINE}(el, f_B, f_T) &= std[BMNA(el, f_B, f_T, t), t], t \in T_{BASELINE} \\ SNR(ch, f_B, f_T, t_E) &= \frac{|\mu_{ACTION}(el, f_B, f_T, t_E) - 1|}{\sigma_{ACTION}(el, f_B, f_T, t_E) + \sigma_{BASELINE}(el, f_B, f_T)}\end{aligned}$$

Note that mean baseline  $BMNA$  is equal to 1 by construction. Frequency band  $SNR$  ( $SNR_{FB}$ ) was defined as:

$$SNR_{FB}(f_B, f_T) = \frac{1}{N_{CAR}} \sum_{el \in CAR} \max_{t_E} \arg[SNR(el, f_B, f_T, t_E)]$$

where  $CAR$  is the subset of electrodes that were used for common average referencing and  $N_{CAR}$  is the number of electrodes in the subset.

The frequency band used for cursor control was selected by identifying the local maximum of  $SNR_{FB}$  with the bottom frequency of the band above 40 Hz (Fig. 3). The electrode used for cursor control was selected among the electrodes with the highest  $SNR_{FB}$  for the selected frequency band.

For *session T7 day 100*, the electrode and the frequency band were selected by first calculating  $SNR_{FB}$  for each individual electrode of the  $CAR$  subset.

$$SNR_{FB}(el, f_B, f_T) = \max_{t_E} \arg[SNR(el, f_B, f_T, t_E)]$$

The electrode with the highest  $SNR_{FB}$  was selected and the frequency band was determined from a local  $SNR_{FB}$  maximum for that individual electrode.

*Contribution of the LWMA filter to the feedback delay.* We empirically measured the contribution of the LWMA filter to the feedback delay as follows. We first simulated the target positions in 100 long test blocks. We sampled the target positions at 1,000 samples per second. We then filtered these target positions using either the 0.4-s- or the 0.8-s-long LWMA filter. For each block and LWMA filter, we calculated the delay that gave the highest correlation between the filtered and unfiltered target positions. We used the mean across the 100 simulated blocks as the contribution of the LWMA filter to the feedback delay.

*Algorithm for detecting action potentials of neurons in the neighborhood of the recording microelectrode.* Wideband MEA recordings from each cursor control session were common average referenced using the mean voltage over the same subset of channels used for common average referencing during that session. Referenced signal from the electrodes used for cursor control was then band-pass filtered in forward and backward direction using the 4th order Butterworth filter with cutoff frequencies of 250 and 7,500 Hz. We then calculated the standard deviation (root-mean-square;  $\sigma$ ) of the filtered signal recorded on each individual electrode. To detect potential spikes recorded on the electrodes used for cursor control, we isolated all instances where filtered signal on that electrode crossed a threshold of  $-3.5\sigma$ . To identify whether these threshold crossings corresponded to spikes of one or several neurons in the neighborhood of the electrode, we used an automated spike-sorting algorithm based on density grid contour clustering and subtractive waveform decomposition (algorithm described in detail in Vargas-Irwin and Donoghue 2007). A brief description of the algorithm follows.

The spike-sorting algorithm projects each isolated threshold crossing, represented by a 48-dimensional vector made of consecutive points of the filtered signal (from 0.5 ms before the crossing until 1.1 ms after the crossing) into two-dimensional space spanned by the first two principal components of all threshold crossings. The density of the projected crossings in this 2D space is then examined using contour clustering to find local maxima. All threshold crossings that fall within the 95-percentile contour of a density maximum are used

to calculate the shape of the potential spike corresponding to that maximum.

To distinguish the spiking of a neuron from random threshold crossings of an oscillatory signal, we required that the amplitude of the shape, defined as the difference between the maximum and the minimum of the shape, was higher than the limit amplitude  $a_{LIM}$  expected from a random oscillatory signal with 95% confidence.  $a_{LIM}$  was calculated as follows. Let us assume that the random oscillatory signal  $x$  is normally distributed with a zero mean and a standard deviation equal to  $\sigma$ . Then every threshold crossing can be seen as a random draw from that distribution with the requirement that the value is lower than the  $-3.5\sigma$ . Thus, the expectation of the minimum of the spike shape  $E(x_{MIN})$  can be estimated as

$$E(x_{MIN}) = \frac{\int_{-\infty}^{-3.5\sigma} \frac{1}{\sigma\sqrt{2\pi}} x e^{-\frac{x^2}{2\sigma^2}} dx}{\Phi(-3.5)} = -\sigma \frac{\phi(-3.5)}{\Phi(-3.5)} = -3.7514\sigma$$

where  $\phi(u)$  and  $\Phi(u)$  are the standard normal probability density function and the corresponding cumulative distribution function:

$$\phi(u) = \frac{1}{\sqrt{2\pi}} e^{-\frac{u^2}{2}} \quad \Phi(u) = \int_{-\infty}^u \phi(t) dt$$

Similarly, the expectation of the maximum of the spike shape  $E(x_{MAX})$  can be estimated as

$$E(x_{MAX}) = \frac{\int_0^{\infty} \frac{1}{\sigma\sqrt{2\pi}} x e^{-\frac{x^2}{2\sigma^2}} dx}{\Phi(\infty) - \Phi(0)} = \sigma \frac{\phi(0) - \phi(\infty)}{\Phi(\infty) - \Phi(0)} = \sqrt{\frac{2}{\pi}} \sigma$$

Thus, assuming the statistical independence of the  $x_{MIN}$  and  $x_{MAX}$ , the expectation of the spike shape amplitude is

$$E(a) = E(x_{MAX} - x_{MIN}) = E(x_{MAX}) - E(x_{MIN}) = 4.5493\sigma$$

Variance of the amplitude can be estimated as

$$\begin{aligned}V(x_{MIN}) &= \frac{\int_{-\infty}^{-3.5\sigma} \frac{1}{\sigma\sqrt{2\pi}} [x - E(x_{MIN})]^2 e^{-\frac{x^2}{2\sigma^2}} dx}{\Phi(-3.5)} \\ &= \left| \begin{array}{l} u = \frac{x}{\sigma} \quad du = \frac{dx}{\sigma} \\ \mu = \frac{E(x_{MIN})}{\sigma} = \sqrt{\frac{2}{\pi}} \end{array} \right| \\ &= \frac{\sigma^2}{\Phi(-3.5)} \int_{-\infty}^{-3.5} (u - \mu)^2 \phi(u) du \\ &= \frac{\sigma^2}{\Phi(-3.5)} [\Phi(u)(1 + \mu^2) + \phi(u)(2\mu - u)]_{-\infty}^{-3.5} \\ &= \frac{\sigma^2}{\Phi(-3.5)} \left[ \Phi(-3.5) \left(1 + \frac{2}{\pi}\right) + \phi(3.5) \left(3.5 + 2\sqrt{\frac{2}{\pi}}\right) \right] \\ &= 20.7528\sigma^2 \\ V(x_{MAX}) &= \frac{\int_0^{\infty} \frac{1}{\sigma\sqrt{2\pi}} (x - E(x_{MAX}))^2 e^{-\frac{x^2}{2\sigma^2}} dx}{\Phi(\infty) - \Phi(0)} \\ &= 2\sigma^2 [\Phi(u)(1 + \mu^2) + \phi(u)(2\mu - u)]_0^{\infty} \\ &= 2\sigma^2 \left[ \frac{1}{2} \left(1 + \frac{2}{\pi}\right) - \frac{2}{\pi} \right] = \sigma^2 \left(1 - \frac{2}{\pi}\right) = 0.3634\sigma^2 \\ V(a) &= V(x_{MIN}) + V(x_{MAX}) = 21.1162\sigma^2\end{aligned}$$

Thus, to claim with 95% confidence that the spike shape amplitude is above the amplitude expected from the random threshold crossings, it has to be higher than

$$a_{LIM} = E(a) + \sqrt{\frac{V(a)}{n}} \cdot t_{stat}(0.05, n - 1)$$

where  $n$  is the number of threshold crossings used to calculate the spike shape and the  $t_{stat}(\alpha, \nu)$  is the statistics for the Student's  $t$  distribution given a right-sided probability  $\alpha$  and  $\nu$  degrees of freedom [for example,  $t_{stat}(0.05, 1, 000) = 1.64$ ].

#### ACKNOWLEDGMENTS

We thank BrainGate2 clinical trial participants T2, T6, and T7 for their dedication to this research.

#### GRANTS

The research was supported by the Morton Cure Paralysis Fund, Office of Research and Development, Rehabilitation R&D Service, Department of Veterans Affairs (B6453R, A6779L, B6459L), NIH: NICHD-NCMRR (N01HD10018), NIDCD (R01DC009899), Doris Duke Charitable Foundation, Stanford Institute for Neuro-Innovation and Translational Neuroscience, Craig H. Neilsen Foundation, MGH-Deane Institute, Katie Samson Foundation, Bio-X NeuroVentures, the Garlick Fund, the Reeve Fund, Institut national de la santé et de la recherche médicale, and the French-American Fulbright Commission.

#### DISCLOSURES

No conflicts of interest, financial or otherwise, are declared by the authors.

#### AUTHOR CONTRIBUTIONS

T.M., D.B., A.A.S., E.E., S.S.C., L.R.H., and J.P.D. conceived and designed research; T.M., D.B., A.A.S., J.S., C.P., B.L.S., C.B., E.M.O., and K.R.T. performed experiments; T.M. analyzed data; T.M., B.Y., K.V.S., J.M.H., L.R.H., and J.P.D. interpreted results of experiments; T.M. prepared figures; T.M. drafted manuscript; T.M., D.B., A.A.S., J.D.S., J.S., C.P., B.Y., K.V.S., J.M.H., L.R.H., and J.P.D. edited and revised manuscript; T.M., D.B., A.A.S., J.D.S., J.S., C.P., B.Y., B.L.S., C.B., E.M.O., K.R.T., E.E., S.S.C., K.V.S., J.M.H., L.R.H., and J.P.D. approved final version of manuscript.

#### REFERENCES

- Affalo T, Kellis S, Klaes C, Lee B, Shi Y, Pejsa K, Shanfield K, Hayes-Jackson S, Aisen M, Heck C, Liu C, Andersen RA. Decoding motor imagery from the posterior parietal cortex of a tetraplegic human. *Science* 348: 906–910, 2015. doi:10.1126/science.aaa5417.
- Ajiboye AB, Simeral JD, Donoghue JP, Hochberg LR, Kirsch RF. Prediction of imagined single-joint movements in a person with high-level tetraplegia. *IEEE Trans Biomed Eng* 59: 2755–2765, 2012. doi:10.1109/TBME.2012.2209882.
- Ajiboye AB, Willett FR, Young DR, Memberg WD, Murphy BA, Miller JP, Walter BL, Sweet JA, Hoyen HA, Keith MW, Peckham PH, Simeral JD, Donoghue JP, Hochberg LR, Kirsch RF. Restoration of reaching and grasping movements through brain-controlled muscle stimulation in a person with tetraplegia: a proof-of-concept demonstration. *Lancet* 389: 1821–1830, 2017. doi:10.1016/S0140-6736(17)30601-3.
- Allen JB. Short term spectral analysis, synthesis, and modification by discrete Fourier transform. *IEEE Transactions Acoust Speech Sig Proc* 25: 235–238, 1977. doi:10.1109/TASSP.1977.1162950.
- Andersen RA, Hwang EJ, Mulliken GH. Cognitive neural prosthetics. *Annu Rev Psychol* 61: 169–190, 2010. doi:10.1146/annurev.psych.093008.100503.
- Andersen RA, Kellis S, Klaes C, Affalo T. Toward more versatile and intuitive cortical brain-machine interfaces. *Curr Biol* 24: R885–R897, 2014. doi:10.1016/j.cub.2014.07.068.
- Bacher D, Jarosiewicz B, Masse NY, Stavisky SD, Simeral JD, Newell K, Oakley EM, Cash SS, Friehs G, Hochberg LR. Neural point-and-click communication by a person with incomplete locked-in syndrome. *Neurorehabil Neural Repair* 29: 462–471, 2015. doi:10.1177/1545968314554624.
- Barrese JC, Rao N, Paroo K, Triebwasser C, Vargas-Irwin C, Franquemont L, Donoghue JP. Failure mode analysis of silicon-based intracortical microelectrode arrays in non-human primates. *J Neural Eng* 10: 066014, 2013. doi:10.1088/1741-2560/10/6/066014.
- Basmajian JV. Control and training of individual motor units. *Science* 141: 440–441, 1963. doi:10.1126/science.141.3579.440.
- Birbaumer N, Ghanayim N, Hinterberger T, Iversen I, Kotchoubey B, Kübler A, Perelmouter J, Taub E, Flor H. A spelling device for the paralysed. *Nature* 398: 297–298, 1999. doi:10.1038/18581.
- Birbaumer N, Ramos Murguialday A, Weber C, Montoya P. Neurofeedback and brain-computer interface clinical applications. *Int Rev Neurobiol* 86: 107–117, 2009. doi:10.1016/S0074-7742(09)86008-X.
- Bouton CE, Shaikhouni A, Annetta NV, Bockbrader MA, Friedenberg DA, Nielson DM, Sharma G, Sederberg PB, Glenn BC, Mysiw WJ, Morgan AG, Deogaonkar M, Rezai AR. Restoring cortical control of functional movement in a human with quadriplegia. *Nature* 533: 247–250, 2016. doi:10.1038/nature17435.
- Bowsher K, Civillico EF, Coburn J, Collinger J, Contreras-Vidal JL, Denison T, Donoghue J, French J, Getzoff N, Hochberg LR, Hoffmann M, Judy J, Kleitman N, Knaack G, Krauthamer V, Ludwig K, Moynahan M, Pancrazio JJ, Peckham PH, Pena C, Pinto V, Ryan T, Saha D, Scharen H, Shermer S, Skodacek K, Takmakov P, Tyler D, Vasudevan S, Wachrathit K, Weber D, Welle CG, Ye M. Brain-computer interface devices for patients with paralysis and amputation: a meeting report. *J Neural Eng* 13: 023001, 2016. doi:10.1088/1741-2560/13/2/023001.
- Buzsáki G, Anastassiou CA, Koch C. The origin of extracellular fields and currents—EEG, ECoG, LFP and spikes. *Nat Rev Neurosci* 13: 407–420, 2012. doi:10.1038/nrn3241.
- Caria A, Sitaram R, Veit R, Begliomini C, Birbaumer N. Volitional control of anterior insula activity modulates the response to aversive stimuli. A real-time functional magnetic resonance imaging study. *Biol Psychiatry* 68: 425–432, 2010. doi:10.1016/j.biopsych.2010.04.020.
- Caria A, Veit R, Sitaram R, Lotze M, Weiskopf N, Grodd W, Birbaumer N. Regulation of anterior insular cortex activity using real-time fMRI. *Neuroimage* 35: 1238–1246, 2007. doi:10.1016/j.neuroimage.2007.01.018.
- Chaudhary U, Birbaumer N, Ramos-Murguialday A. Brain-computer interfaces for communication and rehabilitation. *Nat Rev Neurol* 12: 513–525, 2016. doi:10.1038/nrneurol.2016.113.
- Chestek CA, Gilja V, Nuyujukian P, Foster JD, Fan JM, Kaufman MT, Churchland MM, Rivera-Alvidrez Z, Cunningham JP, Ryu SI, Shenoy KV. Long-term stability of neural prosthetic control signals from silicon cortical arrays in rhesus macaque motor cortex. *J Neural Eng* 8: 045005, 2011. doi:10.1088/1741-2560/8/4/045005.
- Christie BP, Tat DM, Irwin ZT, Gilja V, Nuyujukian P, Foster JD, Ryu SI, Shenoy KV, Thompson DE, Chestek CA. Comparison of spike sorting and thresholding of voltage waveforms for intracortical brain-machine interface performance. *J Neural Eng* 12: 016009, 2015. doi:10.1088/1741-2560/12/1/016009.
- Collinger JL, Wodlinger B, Downey JE, Wang W, Tyler-Kabara EC, Weber DJ, McMorland AJ, Velliste M, Boninger ML, Schwartz AB. High-performance neuroprosthetic control by an individual with tetraplegia. *Lancet* 381: 557–564, 2013. doi:10.1016/S0140-6736(12)61816-9.
- Cunningham JP, Nuyujukian P, Gilja V, Chestek CA, Ryu SI, Shenoy KV. A closed-loop human simulator for investigating the role of feedback control in brain-machine interfaces. *J Neurophysiol* 105: 1932–1949, 2011. doi:10.1152/jn.00503.2010.
- Dickey AS, Suminski A, Amit Y, Hatsopoulos NG. Single-unit stability using chronically implanted multielectrode arrays. *J Neurophysiol* 102: 1331–1339, 2009. doi:10.1152/jn.90920.2008.
- Donoghue JP. Connecting cortex to machines: recent advances in brain interfaces. *Nat Neurosci* 5, Suppl: 1085–1088, 2002. doi:10.1038/nn947.
- Donoghue JP, Nurmikko A, Black M, Hochberg LR. Assistive technology and robotic control using motor cortex ensemble-based neural interface systems in humans with tetraplegia. *J Physiol* 579: 603–611, 2007. doi:10.1113/jphysiol.2006.127209.
- Eccles JC. Interpretation of action potentials evoked in the cerebral cortex. *Electroencephalogr Clin Neurophysiol* 3: 449–464, 1951. doi:10.1016/0013-4694(51)90033-8.
- Engelhard B, Ozeri N, Israel Z, Bergman H, Vaadia E. Inducing  $\gamma$  oscillations and precise spike synchrony by operant conditioning via brain-machine interface. *Neuron* 77: 361–375, 2013. doi:10.1016/j.neuron.2012.11.015.

- Fagg AH, Hatsopoulos NG, de Lafuente V, Moxon KA, Nemati S, Rebesco JM, Romo R, Solla SA, Reimer J, Tkach D, Pohlmeier EA, Miller LE. Biomimetic brain machine interfaces for the control of movement. *J Neurosci* 27: 11842–11846, 2007. doi:10.1523/JNEUROSCI.3516-07.2007.
- Fetz EE. Operant conditioning of cortical unit activity. *Science* 163: 955–958, 1969. doi:10.1126/science.163.3870.955.
- Fetz EE. Volitional control of neural activity: implications for brain-computer interfaces. *J Physiol* 579: 571–579, 2007. doi:10.1113/jphysiol.2006.127142.
- Fetz EE, Wyler AR. Operantly conditioned firing patterns of epileptic neurons in the monkey motor cortex. *Exp Neurol* 40: 586–607, 1973. doi:10.1016/0014-4886(73)90098-8.
- Flint RD, Scheid MR, Wright ZA, Solla SA, Slutzky MW. Long-term stability of motor cortical activity: implications for brain machine interfaces and optimal feedback control. *J Neurosci* 36: 3623–3632, 2016. doi:10.1523/JNEUROSCI.2339-15.2016.
- Flint RD, Wright ZA, Scheid MR, Slutzky MW. Long term, stable brain machine interface performance using local field potentials and multiunit spikes. *J Neural Eng* 10: 056005, 2013. doi:10.1088/1741-2560/10/5/056005.
- Ganguly K, Carmena JM. Emergence of a stable cortical map for neuro-prosthetic control. *PLoS Biol* 7: e1000153, 2009. doi:10.1371/journal.pbio.1000153.
- Ganguly K, Carmena JM. Neural correlates of skill acquisition with a cortical brain-machine interface. *J Mot Behav* 42: 355–360, 2010. doi:10.1080/00222895.2010.526457.
- Gharabaghi A, Naros G, Walter A, Grimm F, Schuermeyer M, Roth A, Bogdan M, Rosenstiel W, Birbaumer N. From assistance towards restoration with epidural brain-computer interfacing. *Restor Neurol Neurosci* 32: 517–525, 2014. doi:10.3233/RNN-140387.
- Gilja V, Chestek CA, Diester I, Henderson JM, Deisseroth K, Shenoy KV. Challenges and opportunities for next-generation intracortically based neural prostheses. *IEEE Trans Biomed Eng* 58: 1891–1899, 2011. doi:10.1109/TBME.2011.2107553.
- Gilja V, Pandarinath C, Blabe CH, Nuyujukian P, Simeral JD, Sarma AA, Sorice BL, Perge JA, Jarosiewicz B, Hochberg LR, Shenoy KV, Henderson JM. Clinical translation of a high-performance neural prosthesis. *Nat Med* 21: 1142–1145, 2015. doi:10.1038/nm.3953.
- Gold C, Henze DA, Koch C, Buzsáki G. On the origin of the extracellular action potential waveform: a modeling study. *J Neurophysiol* 95: 3113–3128, 2006. doi:10.1152/jn.00979.2005.
- Green AM, Kalaska JF. Learning to move machines with the mind. *Trends Neurosci* 34: 61–75, 2011. doi:10.1016/j.tins.2010.11.003.
- Hall TM, Nazarpour K, Jackson A. Real-time estimation and biofeedback of single-neuron firing rates using local field potentials. *Nat Commun* 5: 5462, 2014. doi:10.1038/ncomms6462.
- Heinrich H, Gevensleben H, Strehl U. Annotation: neurofeedback—train your brain to train behaviour. *J Child Psychol Psychiatry* 48: 3–16, 2007. doi:10.1111/j.1469-7610.2006.01665.x.
- Hochberg LR. Turning thought into action. *N Engl J Med* 359: 1175–1177, 2008. doi:10.1056/NEJMcibr0805122.
- Hochberg LR, Bacher D, Jarosiewicz B, Masse NY, Simeral JD, Vogel J, Haddadin S, Liu J, Cash SS, van der Smagt P, Donoghue JP. Reach and grasp by people with tetraplegia using a neurally controlled robotic arm. *Nature* 485: 372–375, 2012. doi:10.1038/nature11076.
- Hochberg LR, Serruya MD, Friehs GM, Mukand JA, Saleh M, Caplan AH, Branner A, Chen D, Penn RD, Donoghue JP. Neuronal ensemble control of prosthetic devices by a human with tetraplegia. *Nature* 442: 164–171, 2006. doi:10.1038/nature04970.
- Hu K, Chen C, Meng Q, Williams Z, Xu W. Scientific profile of brain-computer interfaces: bibliometric analysis in a 10-year period. *Neurosci Lett* 635: 61–66, 2016. doi:10.1016/j.neulet.2016.10.022.
- Hwang EJ, Bailey PM, Andersen RA. Volitional control of neural activity relies on the natural motor repertoire. *Curr Biol* 23: 353–361, 2013. doi:10.1016/j.cub.2013.01.027.
- Jackson A, Fetz EE. Interfacing with the computational brain. *IEEE Trans Neural Syst Rehabil Eng* 19: 534–541, 2011. doi:10.1109/TNSRE.2011.2158586.
- Jarosiewicz B, Chase SM, Fraser GW, Velliste M, Kass RE, Schwartz AB. Functional network reorganization during learning in a brain-computer interface paradigm. *Proc Natl Acad Sci USA* 105: 19486–19491, 2008. doi:10.1073/pnas.0808113105.
- Jarosiewicz B, Sarma AA, Bacher D, Masse NY, Simeral JD, Sorice B, Oakley EM, Blabe C, Pandarinath C, Gilja V, Cash SS, Eskandar EN, Friehs G, Henderson JM, Shenoy KV, Donoghue JP, Hochberg LR. Virtual typing by people with tetraplegia using a self-calibrating intracortical brain-computer interface. *Sci Transl Med* 7: 313ra179, 2015. doi:10.1126/scitranslmed.aac7328.
- Jerbi K, Freyermuth S, Minotti L, Kahane P, Berthoz A, Lachaux JP. Watching brain TV and playing brain ball exploring novel BCI strategies using real-time analysis of human intracranial data. *Int Rev Neurobiol* 86: 159–168, 2009. doi:10.1016/S0074-7742(09)86012-1.
- Kajikawa Y, Schroeder CE. How local is the local field potential? *Neuron* 72: 847–858, 2011. doi:10.1016/j.neuron.2011.09.029.
- Kao JC, Stavisky SD, Sussillo D, Nuyujukian P, Shenoy KV. Information systems opportunities in brain-machine interface decoders. *Proc IEEE* 102: 666–682, 2014. doi:10.1109/JPROC.2014.2307357.
- Katzner S, Nauhaus I, Benucci A, Bonin V, Ringach DL, Carandini M. Local origin of field potentials in visual cortex. *Neuron* 61: 35–41, 2009. doi:10.1016/j.neuron.2008.11.016.
- Kennedy PR, Bakay RA, Moore MM, Adams K, Goldwaithe J. Direct control of a computer from the human central nervous system. *IEEE Trans Rehabil Eng* 8: 198–202, 2000. doi:10.1109/86.847815.
- Kennedy PR, Kirby MT, Moore MM, King B, Mallory A. Computer control using human intracortical local field potentials. *IEEE Trans Neural Syst Rehabil Eng* 12: 339–344, 2004. doi:10.1109/TNSRE.2004.834629.
- Kim SP, Simeral JD, Hochberg LR, Donoghue JP, Black MJ. Neural control of computer cursor velocity by decoding motor cortical spiking activity in humans with tetraplegia. *J Neural Eng* 5: 455–476, 2008. doi:10.1088/1741-2560/5/4/010.
- Kübler A, Kotchoubey B, Hinterberger T, Ghanayim N, Perelmouter J, Schauer M, Fritsch C, Taub E, Birbaumer N. The thought translation device: a neurophysiological approach to communication in total motor paralysis. *Exp Brain Res* 124: 223–232, 1999. doi:10.1007/s002210050617.
- Kübler A, Nijboer F, Mellinger J, Vaughan TM, Pawelzik H, Schalk G, McFarland DJ, Birbaumer N, Wolpaw JR. Patients with ALS can use sensorimotor rhythms to operate a brain-computer interface. *Neurology* 64: 1775–1777, 2005. doi:10.1212/01.WNL.0000158616.43002.6D.
- Leach JB, Achyuta AK, Murthy SK. Bridging the divide between neuro-prosthetic design, tissue engineering and neurobiology. *Front Neuroeng* 2: 18, 2010. doi:10.3389/fneuro.16.018.2009.
- Leins U, Goth G, Hinterberger T, Klinger C, Rumpf N, Strehl U. Neuro-feedback for children with ADHD: a comparison of SCP and Theta/Beta protocols. *Appl Psychophysiol Biofeedback* 32: 73–88, 2007. doi:10.1007/s10484-007-9031-0.
- Lorente de No R. Analysis of the distribution of the action currents of nerve in volume conductors. *Stud Rockefeller Inst Med Res Repr* 132: 384–477, 1947.
- McFarland DJ, Sarnacki WA, Vaughan TM, Wolpaw JR. Brain-computer interface (BCI) operation: signal and noise during early training sessions. *Clin Neurophysiol* 116: 56–62, 2005. doi:10.1016/j.clinph.2004.07.004.
- Mehring C, Rickert J, Vaadia E, Cardoso de Oliveira S, Aertsen A, Rotter S. Inference of hand movements from local field potentials in monkey motor cortex. *Nat Neurosci* 6: 1253–1254, 2003. doi:10.1038/nm1158.
- Mellinger J, Schalk G, Braun C, Preissl H, Rosenstiel W, Birbaumer N, Kübler A. An MEG-based brain-computer interface (BCI). *Neuroimage* 36: 581–593, 2007. doi:10.1016/j.neuroimage.2007.03.019.
- Milekovic T, Ball T, Schulze-Bonhage A, Aertsen A, Mehring C. Error-related electrocorticographic activity in humans during continuous movements. *J Neural Eng* 9: 026007, 2012. doi:10.1088/1741-2560/9/2/026007.
- Milekovic T, Sarma AA, Bacher D, Simeral JD, Saab J, Pandarinath C, Sorice BL, Blabe C, Oakley EM, Tringale KR, Eskandar E, Cash SS, Henderson JM, Shenoy KV, Donoghue JP, Hochberg LR. Stable long-term BCI-enabled communication in ALS and locked-in syndrome using LFP signals. *J Neurophysiol* 120: 343–360, 2018. doi:10.1152/jn.00493.2017.
- Milekovic T, Truccolo W, Grün S, Riehle A, Brochier T. Local field potentials in primate motor cortex encode grasp kinetic parameters. *Neuroimage* 114: 338–355, 2015. doi:10.1016/j.neuroimage.2015.04.008.
- Miralles F, Vargiu E, Dauwalder S, Solà M, Müller-Putz G, Wriessnegger SC, Pinegger A, Kübler A, Halder S, Käthner I, Martin S, Daly J, Armstrong E, Guger C, Hintermüller C, Lowish H. Brain computer interface on track to home. *ScientificWorldJournal* 2015: 623896, 2015. doi:10.1155/2015/623896.
- Mollazadeh M, Aggarwal V, Davidson AG, Law AJ, Thakor NV, Schieber MH. Spatiotemporal variation of multiple neurophysiological signals in the primary motor cortex during dexterous reach-to-grasp movements. *J Neurosci* 31: 15531–15543, 2011. doi:10.1523/JNEUROSCI.2999-11.2011.

- Moore DS, McCabe GP, Craig B. *Introduction to the Practice of Statistics*. Basingstoke, UK: Freeman, 2009.
- Moritz CT, Fetz EE. Volitional control of single cortical neurons in a brain-machine interface. *J Neural Eng* 8: 025017, 2011. doi:10.1088/1741-2560/8/2/025017.
- Moritz CT, Perlmutter SI, Fetz EE. Direct control of paralysed muscles by cortical neurons. *Nature* 456: 639–642, 2008. doi:10.1038/nature07418.
- Nicolelis MA, Lebedev MA. Principles of neural ensemble physiology underlying the operation of brain-machine interfaces. *Nat Rev Neurosci* 10: 530–540, 2009. doi:10.1038/nrn2653.
- Nijboer F, Furdea A, Gunst I, Mellinger J, McFarland DJ, Birbaumer N, Kübler A. An auditory brain-computer interface (BCI). *J Neurosci Methods* 167: 43–50, 2008. doi:10.1016/j.jneumeth.2007.02.009.
- Nishimura Y, Perlmutter SI, Fetz EE. Restoration of upper limb movement via artificial corticospinal and musculoskeletal connections in a monkey with spinal cord injury. *Front Neural Circuits* 7: 57, 2013. doi:10.3389/fncir.2013.00057.
- Nuyujukian P, Kao JC, Fan JM, Stavisky SD, Ryu SI, Shenoy KV. Performance sustaining intracortical neural prostheses. *J Neural Eng* 11: 066003, 2014. doi:10.1088/1741-2560/11/6/066003.
- Pandarinath C, Nuyujukian P, Blabe CH, Sorice BL, Saab J, Willett FR, Hochberg LR, Shenoy KV, Henderson JM. High performance communication by people with paralysis using an intracortical brain-computer interface. *eLife* 6: e18554, 2017. doi:10.7554/eLife.18554.
- Perge JA, Homer ML, Malik WQ, Cash S, Eskandar E, Friehs G, Donoghue JP, Hochberg LR. Intra-day signal instabilities affect decoding performance in an intracortical neural interface system. *J Neural Eng* 10: 036004, 2013. doi:10.1088/1741-2560/10/3/036004.
- Perge JA, Zhang S, Malik WQ, Homer ML, Cash S, Friehs G, Eskandar EN, Donoghue JP, Hochberg LR. Reliability of directional information in unsorted spikes and local field potentials recorded in human motor cortex. *J Neural Eng* 11: 046007, 2014. doi:10.1088/1741-2560/11/4/046007.
- Pesaran B. Uncovering the mysterious origins of local field potentials. *Neuron* 61: 1–2, 2009. doi:10.1016/j.neuron.2008.12.019.
- Pfurtscheller G, Neuper C, Müller GR, Obermaier B, Krausz G, Schlögl A, Scherer R, Graimann B, Keirath C, Skliris D, Wörtz M, Supp G, Schrank C. Graz-BCI: state of the art and clinical applications. *IEEE Trans Neural Syst Rehabil Eng* 11: 177–180, 2003. doi:10.1109/TNSRE.2003.814454.
- Polikov VS, Tresco PA, Reichert WM. Response of brain tissue to chronically implanted neural electrodes. *J Neurosci Methods* 148: 1–18, 2005. doi:10.1016/j.jneumeth.2005.08.015.
- Rickert J, Oliveira SC, Vaadia E, Aertsen A, Rotter S, Mehring C. Encoding of movement direction in different frequency ranges of motor cortical local field potentials. *J Neurosci* 25: 8815–8824, 2005. doi:10.1523/JNEUROSCI.0816-05.2005.
- Rockstroh B, Elbert T, Birbaumer N, Lutzenberger W. Biofeedback-produced hemispheric asymmetry of slow cortical potentials and its behavioural effects. *Int J Psychophysiol* 9: 151–165, 1990. doi:10.1016/0167-8760(90)90069-P.
- Sadtler PT, Quick KM, Golub MD, Chase SM, Ryu SI, Tyler-Kabara EC, Yu BM, Batista AP. Neural constraints on learning. *Nature* 512: 423–426, 2014. doi:10.1038/nature13665.
- Schalk G, Miller KJ, Anderson NR, Wilson JA, Smyth MD, Ojemann JG, Moran DW, Wolpaw JR, Leuthardt EC. Two-dimensional movement control using electrocorticographic signals in humans. *J Neural Eng* 5: 75–84, 2008. doi:10.1088/1741-2560/5/1/008.
- Schroeder KE, Chestek CA. Intracortical brain-machine interfaces advance sensorimotor neuroscience. *Front Neurosci* 10: 291, 2016. doi:10.3389/fnins.2016.00291.
- Schwartz AB, Cui XT, Weber DJ, Moran DW. Brain-controlled interfaces: movement restoration with neural prosthetics. *Neuron* 52: 205–220, 2006. doi:10.1016/j.neuron.2006.09.019.
- Shenoy KV, Carmena JM. Combining decoder design and neural adaptation in brain-machine interfaces. *Neuron* 84: 665–680, 2014. doi:10.1016/j.neuron.2014.08.038.
- Simeral JD, Kim SP, Black MJ, Donoghue JP, Hochberg LR. Neural control of cursor trajectory and click by a human with tetraplegia 1000 days after implant of an intracortical microelectrode array. *J Neural Eng* 8: 025027, 2011. doi:10.1088/1741-2560/8/2/025027.
- Sollfrank T, Ramsay A, Perdakis S, Williamson J, Murray-Smith R, Leeb R, Millán JDR, Kübler A. The effect of multimodal and enriched feedback on SMR-BCI performance. *Clin Neurophysiol* 127: 490–498, 2016. doi:10.1016/j.clinph.2015.06.004.
- Stavisky SD, Kao JC, Nuyujukian P, Ryu SI, Shenoy KV. A high performing brain-machine interface driven by low-frequency local field potentials alone and together with spikes. *J Neural Eng* 12: 036009, 2015. doi:10.1088/1741-2560/12/3/036009.
- Taylor DM, Tillery SI, Schwartz AB. Direct cortical control of 3D neuroprosthetic devices. *Science* 296: 1829–1832, 2002. doi:10.1126/science.1070291.
- Tsu AP, Burish MJ, GodLove J, Ganguly K. Cortical neuroprosthetics from a clinical perspective. *Neurobiol Dis* 83: 154–160, 2015. doi:10.1016/j.nbd.2015.07.015.
- Vansteensel MJ, Pels EGM, Bleichner MG, Branco MP, Denison T, Freudenburg ZV, Gosselaar P, Leinders S, Ottens TH, Van Den Boom MA, Van Rijen PC, Aarnoutse EJ, Ramsey NF. Fully implanted brain-computer interface in a locked-in patient with ALS. *N Engl J Med* 375: 2060–2066, 2016. doi:10.1056/NEJMoa1608085.
- Vargas-Irwin C, Donoghue JP. Automated spike sorting using density grid contour clustering and subtractive waveform decomposition. *J Neurosci Methods* 164: 1–18, 2007. doi:10.1016/j.jneumeth.2007.03.025.
- Vukelić M, Gharabaghi A. Oscillatory entrainment of the motor cortical network during motor imagery is modulated by the feedback modality. *Neuroimage* 111: 1–11, 2015. doi:10.1016/j.neuroimage.2015.01.058.
- Waldert S, Lemon RN, Kraskov A. Influence of spiking activity on cortical local field potentials. *J Physiol* 591: 5291–5303, 2013. doi:10.1113/jphysiol.2013.258228.
- Wang D, Zhang Q, Li Y, Wang Y, Zhu J, Zhang S, Zheng X. Long-term decoding stability of local field potentials from silicon arrays in primate motor cortex during a 2D center out task. *J Neural Eng* 11: 036009, 2014. doi:10.1088/1741-2560/11/3/036009.
- Wang W, Collinger JL, Perez MA, Tyler-Kabara EC, Cohen LG, Birbaumer N, Brose SW, Schwartz AB, Boninger ML, Weber DJ. Neural interface technology for rehabilitation: exploiting and promoting neuroplasticity. *Phys Med Rehabil Clin N Am* 21: 157–178, 2010. doi:10.1016/j.pmr.2009.07.003.
- Weiskopf N. Real-time fMRI and its application to neurofeedback. *Neuroimage* 62: 682–692, 2012. doi:10.1016/j.neuroimage.2011.10.009.
- Weiskopf N, Mathiak K, Bock SW, Scharnowski F, Veit R, Grodd W, Goebel R, Birbaumer N. Principles of a brain-computer interface (BCI) based on real-time functional magnetic resonance imaging (fMRI). *IEEE Trans Biomed Eng* 51: 966–970, 2004. doi:10.1109/TBME.2004.827063.
- Weiskopf N, Veit R, Erb M, Mathiak K, Grodd W, Goebel R, Birbaumer N. Physiological self-regulation of regional brain activity using real-time functional magnetic resonance imaging (fMRI): methodology and exemplary data. *Neuroimage* 19: 577–586, 2003. doi:10.1016/S1053-8119(03)00145-9.
- Weyand S, Takehara-Nishiuchi K, Chau T. Weaning off mental tasks to achieve voluntary self-regulatory control of a near-infrared spectroscopy brain-computer interface. *IEEE Trans Neural Syst Rehabil Eng* 23: 548–561, 2015. doi:10.1109/TNSRE.2015.2399392.
- Wodlinger B, Downey JE, Tyler-Kabara EC, Schwartz AB, Boninger ML, Collinger JL. Ten-dimensional anthropomorphic arm control in a human brain-machine interface: difficulties, solutions, and limitations. *J Neural Eng* 12: 016011, 2015. doi:10.1088/1741-2560/12/1/016011.
- Wolpaw JR, McFarland DJ, Neat GW, Forneris CA. An EEG-based brain-computer interface for cursor control. *Electroencephalogr Clin Neurophysiol* 78: 252–259, 1991. doi:10.1016/0013-4694(91)90040-B.
- Wolpaw JR, Wolpaw EW. *Brain-Computer Interfaces: Principles and Practice*. Oxford, UK: Oxford University Press, 2012.
- Xing D, Yeh CI, Shapley RM. Spatial spread of the local field potential and its laminar variation in visual cortex. *J Neurosci* 29: 11540–11549, 2009. doi:10.1523/JNEUROSCI.2573-09.2009.
- Yaffee RA, McGee M. *Introduction to Time Series Analysis and Forecasting: With Applications of SAS and SPSS*. San Diego, CA: Academic, 2000, p. 528.
- Yousry TA, Schmid UD, Alkadhi H, Schmidt D, Peraud A, Buettner A, Winkler P. Localization of the motor hand area to a knob on the precentral gyrus. A new landmark. *Brain* 120: 141–157, 1997. doi:10.1093/brain/120.1.141.
- Zanos TP, Mineault PJ, Pack CC. Removal of spurious correlations between spikes and local field potentials. *J Neurophysiol* 105: 474–486, 2011. doi:10.1152/jn.00642.2010.